Polyprodrug Amphiphiles: Hierarchical Assemblies for Shape-Regulated Cellular Internalization, Trafficking and Drug Delivery

Xianglong Hu,[†] Jinming Hu,*[,†] Jie Tian,[‡] Zhishen Ge,[†] Guoying Zhang,[†] Kaifu Luo,[†] and Shiyong Liu*[,†]

[†] *CAS Key Laboratory of Soft Matter Chemistry, Hefei National Laboratory for Physical Sciences at the Microscale, Department of Polymer Science and Engineering, University of Science and Technology of China, Hefei, Anhui 230026, China*

[‡] *Engineering and Materials Science Experiment Center, University of Science and Technology of China, Hefei 230027, China*

***** To whom correspondence should be addressed.

E-mail: sliu@ustc.edu.cn; hjm85@mail.ustc.edu.cn

Table of Contents

Experimental Section

Materials

Poly(ethylene oxide) monomethyl ether (PEG_{45}-OH, M_n = 2.0 kDa, M_w/M_n = 1.06), (*S*)-(+)-camptothecin (CPT), DL-dithiothreitol (DTT), doxorubicin hydrochloride (Dox·HCl), 2-deoxyglucose (DOG), methyl-*β*-cyclodextran (M*β*CD), amiloride hydrochloride, sucrose, sodium azide (NaN_3), and 2, 2'-dithiodiethanol were purchased from Sigma-Aldrich and used as received. 2, 2'-Azobis(2-methylpropionitrile) (AIBN) was obtained from Acros chemicals and recrystallized from 95% ethanol. Dichloromethane (DCM) was distilled over CaH_2 and tetrahydrafuran (THF) was distilled over sodium shavings. Diethyl ether, 4-dimethyaminopyridine (DMAP), ethyl acetate, petroleum ether, and all other reagents were purchased from Sinopharm Chemical Reagent Co. Ltd. and used as received. Water used in this study was deionized with a Milli-QSP reagent water system (Millipore) to a specific resistivity of 18.4 MΩ·cm. Lysotracker Red, Mitotracker Green, Actin-Tracker Green and Tubulin-Tracker Red were purchased from Molecular Probes. Fetal bovine serum (FBS), penicillin, streptomycin, and Dulbecco's modified Eagle's medium (DMEM) were obtained from GIBCO and used as received. Bovine serum albumin (BSA), 1,10-dioctadecyl-3,3,30,30-tetramethylindocarbocyanine perchlorate (Dil), 3,30-dioctadecyloxacarbocyanine perchlorate (DiO), and DRAQ5™ were purchased from Invitrogen. PEG_{45}-based RAFT agent[1] and fluorescent dye-containing monomer, 4-(2-methylacryloyloxyethylamino)-7-nitro-2,1,3-benzoxadiazole (NBD)[2] were synthesized according to literature procedures.

Characterization

All nuclear magnetic resonance (NMR) spectra were recorded on a Bruker AV300 NMR spectrometer (resonance frequency of 300 MHz for ^1H) operated in the Fourier transform mode. $CDCl_3$ was used as the solvent. Molecular weights and molecular weight distributions were determined by GPC using a series of three linear Styragel columns HR2, HR4, HR5 and an oven temperature of 45 ^oC. Waters 1515 pump and Waters 2414 differential refractive index detector (set at 30 ^oC) was used. The eluent was DMF at a flow rate of 1.0 mL/min. A series of six polystyrene standards with molecular weights ranging from 800 to 400,000 g/mol were used for calibration. Fluorescence spectra were recorded on F-4600 (Hitachi)

spectrofluorometer (slit widths: Ex. 5 nm, Em. 5 nm). The transmittance curves and UV-vis absorption spectra were acquired on a Unico UV/vis 2802PCS spectrophotometer. Circular dichroism (CD) spectra were acquired on a J-810 spectropolarimeter (JASCO). Laser light scattering (LLS) measurements were conducted on a commercial spectrometer (ALV/DLS/ SLS-5022F) equipped with a multi-tau digital time correlator (ALV5000) and a cylindrical 22 mW UNIPHASE He-Ne laser (λ_0= 632.8 nm) as the light source. In dynamic LLS, scattered light was collected at a fixed angle of 90^o for duration of ~5 min. Distribution averages and particle size distributions were computed using cumulants analysis and CONTIN routines. In static LLS, scattered light was collected from the angle of 20^o to 150^o for each sample. Data were averaged over three measurements. All samples were filtered through 1.2 μm Millipore Acrodisc-12 filters to remove dust. TEM measurements were conducted on a JEOL 2010 electron microscope. Unless otherwise stated, the sample for TEM observations was prepared by placing 10 μL self-assembly dispersion on copper grids, followed by immediate freeze drying under vacuum to keep the morphological structure in situ. AFM measurements were performed on a Bruker (Digital Instruments) Multimode Nanoscope IIID operating in the tapping mode under ambient conditions. Silicon cantilever (RFESP) with resonance frequency of ~80 kHz and spring constant of ~3 N/m was used. The set-point amplitude ratio was maintained at 0.7 to minimize sample deformation induced by the tip. The samples were prepared by dip coating 0.05 g/L aqueous micellar solutions onto the surface of freshly cleaved mica. Field-emission scanning electron microscope (FE-SEM) observations were conducted on a high-resolution JEOL JSM-6700 field-emission scanning electron microscopy. The samples for SEM observations were prepared by placing 10 μL of self-assembly dispersion on copper grids successively coated with thin films of Formvar and carbon. Differential scanning calorimetry analysis was carried out using a TA Q200 differential scanning calorimeter (TA Instruments, USA). The samples were first heated to 180 °C at 10 °C/min from -50 °C, kept there for 10 min to eliminate thermal histories, and then cooled to −50 °C at a cooling rate of 5 °C/min. Afterwards, the second heating scans at a heating rate of 10 °C/min were carried out. X-ray powder diffraction patterns (XRD) were obtained on a Philips X'Pert PRO X-ray diffractometer. Flow cytometric analysis was conducted using a BD FACSCalibur flow cytometer with the excitation wavelength set to be 488 nm. Confocal laser

scanning microscopy (CLSM) images were acquired using Leica TCS SP5 microscope. Reversed-phase HPLC (RP-HPLC) analysis was performed on a Shimadzu HPLC system, equipped with a LC-20AP binary pump, a SPD-20A UV-Vis detector, and a Symmetry C18 column. UV-Vis detector was set at 370 nm for data collection and analysis.

Methods

Synthetic routes employed for the preparation of reduction-responsive CPT monomer (CPTM) and PEG-*b*-PCPTM polyprodrug amphiphiles are shown in Scheme 1b.

Synthesis of 2-((2-hydroxyethyl)disulfanyl)ethyl methacrylate (HSEMA). HSEMA was synthesized by mono-esterfication of 2,2'-dithiodiethanol with methacryloyl chloride. Typically, triethylamine (6.07g, 60 mmol), 2,2'-dithiodiethanol (6.16 g, 40 mmol), and dry THF (200 mL) were charged into a 500 mL round-bottom flask, cooled to 0 ^{o}C in an ice-water bath, and then methacryloyl chloride (4.18 g, 40 mmol) in 100 mL dry THF was added dropwise over a period of 1 h under vigorous magnetic stirring. After the addition was completed, the reaction mixture was stirred at room temperature overnight. After filtration and evaporating all the solvents, the residues were diluted with ethyl acetate and washed twice with water and brine, respectively. The organic layer was dried over anhydrous $MgSO_4$, filtered, concentrated and finally purified by silica gel column chromatograph using ethyl acetate/petroleum ether (1/3 v/v) as the eluent, affording HSEMA as a yellowish liquid (7.43 g, yield: 71.6%). ^{1}H NMR spectrum labeled with protons assignment was presented in Figure S1a. ^{1}H NMR ($CDCl_3$, δ, ppm, TMS): 6.14 (s, 1H), 5.61 (s, 1H), 4.43 (t, J = 6.7 Hz, 2H), 3.90 (t, J = 5.8 Hz, 2H), 2.98 (t, J = 6.7 Hz, 2H), 2.89 (t, J = 5.8 Hz, 2H), 1.95 (s, 3H).

Synthesis of reduction-responsive CPT monomer (CPTM). Typical procedures for the synthesis of CPTM are as follows. Camptothecin (CPT, 2.0 g, 5.74 mmol) and DMAP (2.11 g, 17.3 mmol) were suspended in dry DCM (50 mL) under argon atmosphere. Triphosgene (0.567 g, 1.92 mmol) was added and the mixture was stirred for 30 min at room temperature. HSEMA (1.40 g, 6.31 mmol, in 15 mL dry THF) was added dropwise via a constant pressure funnel. The reaction mixture was stirred overnight during which a white precipitate was formed. After filtration and evaporating all the solvents, the residues were diluted with diethyl acetate and washed once with water, twice with 1.0 M HCl, and twice with brine, respectively.

The organic layer was dried over anhydrous $MgSO_4$, filtered, and concentrated on a rotary evaporator. The crude product was purified by column chromatography using ethyl acetate as eluent (100% EtOAc, TLC R_f = 0.63, visualize under UV light) to give CPTM as a pale solid powder (2.92 g, yield: 86%). ^{1}H NMR, ^{13}C-NMR, APCI-MS and RP-HPLC analyses of CPTM were shown in Figure S1b-e. ^{1}H NMR ($CDCl_3$, δ, ppm, TMS): 8.41 (s, 1H), 8.23 (d, J = 11.3 Hz, 1H), 7.95 (d, J = 10.8 Hz, 1H), 7.91 – 7.81 (m, 1H), 7.81 – 7.58 (m, 1H), 7.35 (s, 1H), 6.08 (s, 1H), 5.56 (s, 1H), 5.40 (d, 2H), 5.34 (d, J = 23.6 Hz, 2H), 4.60 – 4.24 (m, 4H), 2.94 (m, J = 14.0, 8.7 Hz, 4H), 1.97 – 1.65 (m, 5H), 1.12 – 0.87 (m, 3H). ^{13}C NMR ($CDCl_3$, δ, ppm, TMS): 167.25, 167.05, 157.31, 153.46, 152.32, 148.92, 146.52, 145.62, 135.98, 131.17, 130.73, 129.70, 128.48, 128.20, 128.11, 125.97, 120.29, 95.97, 78.05, 67.09, 66.56, 62.42, 50.02, 37.29, 36.6, 31.91, 18.24, 7.64. APCI-MS: m/z calc. for $C_{29}H_{28}N_2O_8S_2$ 597.13; found 597.14 $[M+H]^+$. RP-HPLC analysis: elution peak at 7.05 min (80/20, CH_3OH/H_2O, λ = 370 nm). By employing similar protocols, a control molecule for CPTM without unsaturated C=C bond, CCPTM, was also synthesized to investigate the reduction milieu-responsiveness of CPTM (Figure S17a). ^{1}H NMR ($CDCl_3$, δ, ppm, TMS): 8.41 (s, 1H), 8.24 (d, J = 8.4 Hz, 1H), 7.96 (d, J = 8.1 Hz, 1H), 7.90 – 7.78 (m, 1H), 7.69 (t, J = 7.5 Hz, 1H), 7.35 (s, 1H), 5.40 (d, J = 17.3 Hz, 2H), 5.31 (s, 2H), 4.38 (t, J = 7.6, 4.6 Hz, 2H), 4.26 (t, J = 6.5 Hz, 2H), 3.05 – 2.81 (m, 4H), 2.03 (s, 3H), 1.91 (q, 2H), 1.02 (t, 3H). APCI-MS: m/z calc. for $C_{27}H_{26}N_2O_8S_2$ 570.11; found 571.13 $[M+H]^+$. RP-HPLC analysis: 6.01 min (80/20, CH_3OH/H_2O, λ = 370 nm).

Synthesis of PEG-b-PCPTM polyprodrug amphiphiles. Reversible addition-fragmentation chain transfer (RAFT) polymerization technique was employed for the synthesis of PEG-*b*-PCPTM polyprodrug amphiphiles.[3] Typically, PEG-based RAFT agent (46 mg, 0.02 mmol), CPTM (632 mg, 1.06 mmol), and AIBN (0.33 mg, 0.002 mmol) were charged into a glass ampoule containing 6 mL 1,4-dioxane and DMSO mixed solvents (1:1, v/v). The ampoule was then degassed via three freeze-pump-thaw cycles and flame-sealed under vacuum. It was then immersed into an oil bath thermostated at 70 ^{o}C to start the polymerization. After 24 h, the ampoule was quenched into liquid nitrogen to terminate the polymerization. The mixture was precipitated into an excess of diethyl ether to generate pale residues, the residues were dissolved in DCM and precipitated into diethyl ether. The product

was further treated with an excess of AIBN (20 equiv.) in DCM to remove terminal trithiocarbonate moieties. After stirring at 60 °C for 6 h, the solution was precipitated into an excess of diethyl ether, and the above dissolution-precipitation cycle was repeated for three times. The final product was dried in a vacuum oven overnight at room temperature, yielding a pale solid powder (654.9 mg, yield: 96.6 %). The molecular weight and molecular weight distribution of PEG-*b*-PCPTM were determined by GPC using DMF as the eluent, revealing an M_n of 32.6 kDa and M_w/M_n of 1.23 (Figure S2b). The actual degree of polymerization (DP) of the PEG-*b*-PCPTM was determined to be 52 by ^{1}H NMR analysis recorded in $CDCl_3$. The obtained polyprodrug amphiphiles were denoted as PEG_{45}-*b*-$PCPTM_{52}$. Following similar procedures, PEG_{45}-*b*-$PCPTM_{87}$, PEG_{45}-*b*-$PCPTM_{24}$, and NBD-labelled PEG_{45}-*b*-$P(CPTM_{0.99}$-*co*-$NBD_{0.01})_{33}$[4] polyprodrug amphiphiles were also synthesized. The structural parameters of all polyprodrug amphiphiles are summarized in Table 1.

Self-assembly of PEG-b-PCPTM polyprodrug amphiphiles. Typical self-assembly procedures employed for four types of nanostructures are as follows. For smooth disks, PEG-*b*-PCPTM (2.0 mg) was dissolved in 1.0 mL DMSO overnight under magnetic stirring at a rate of 1000 rpm, deionized water (9 mL) was then added dropwise at a rate of 8.0 mL/h via a syringe pump. The stirring rate was fixed at 1000 rpm in all cases and the temperature was fixed at 25 ^oC during the self-assembly process. The colloidal dispersion was further stirred for another 2 h, followed by dialysis (MW cutoff, 3.5 kDa) against deionized water for 12 h to remove organic solvent. During this process, fresh deionized water was replaced approximately every 2 h.

For staggered lamellae, PEG-*b*-PCPTM (2.0 mg) was dissolved in 1.0 mL 1,4-dioxane overnight under stirring at a rate of 1000 rpm, deionized water (9 mL) was then added dropwise at a rate of 8.0 mL/h. The stirring rate was fixed at 1000 rpm in all cases and the temperature was fixed at 25 ^oC during the self-assembling process. The colloidal dispersion was further stirred for another 2 h, followed by dialysis (MW cutoff, 3.5 kDa) against deionized water for 12 h to remove organic solvent. During this process, fresh deionized water was replaced approximately every 2 h.

For LCVs, the preparation procedures were identical to those for staggered lamellae nanostructures except that the water adding rate was 0.5 mL/h. Dox·HCl-loaded LCVs were

fabricated as follows. PEG-*b*-PCPTM was dissolved in 1.0 mL 1,4-dioxane overnight under stirring at a rate of 1000 rpm, aqueous solution of Dox·HCl was then added dropwise at a rate of 0.5 mL/h. After stirring for 2 h, the solution was transferred into a dialysis tube (MW cutoff, 3.5 kDa) and dialyzed against water for 24 h. Fresh deionized water was replaced every 2 h.

For spheres, PEG-*b*-PCPTM (2.0 mg) was first dissolved in 1.0 mL DMSO, and then quickly injected into 9 mL deionized water in one shot under vigorous stirring. The colloidal dispersion was further stirred for another 2 h, followed by dialysis (MW cutoff, 3.5 kDa) against deionized water for 12 h to remove DMSO. During this process, fresh deionized water was replaced approximately every 2 h.

Effect of water content on microstructural evolution of PEG_{45}-b-$PCPTM_{52}$ assemblies. Optical transmittance measurement was performed according to published procedures. PEG_{45}-*b*-$PCPTM_{52}$ was first dissolved in the corresponding common organic solvent, deionized water was then added dropwise at the respective water addition rate with constant magnetic stirring rate as described in the methods section. At predetermined water content, the water addition was paused and the dispersion was left to equilibrate for 30 min. The transmittance was then measured at a wavelength of 800 nm with an UV/vis spectrophotometer. The cycle of water addition, equilibration, and transmittance measurement was continued until the change in optical transmittance upon water addition was very small.

To investigate the water content dependent morphological transition for self-assembled nanostructures of PEG_{45}-*b*-$PCPTM_{52}$ polyprodrug amphiphiles at varying intermediate water contents during the self-assembly process, the colloidal dispersion at predetermined water content points was withdrawn and deposited onto carbon coated TEM copper grids, followed with immediate freeze drying under vacuum for TEM measurements.

Form factor fitting for smooth disks. The orientationally averaged form factor for a disk of diameter *d* and thickness *h* is given as[5,6]

$$P(K) = \int_0^{\pi/2} \frac{\sin^2(K(h/2)\cos\theta)}{(K(h/2)\cos\theta)^2} \frac{4J_1^2(K(d/2)\sin\theta)}{(K(d/2)\sin\theta)^2} \sin\theta \mathrm{d}\theta. \quad (1)$$

Here, $J_1(x) = \frac{\sin x}{x^2} - \frac{\cos x}{x}$ is the first order Bessel function, and $K = (4\pi n/\lambda)\sin(\theta/2)$ is the scattering wave vector, with *n* being the refractive index of the medium, λ the wavelength

of the incident light in vacuum, and θ the scattering angle. For polydisperse cylinders or disks with the probability density function for the particle diameter and thickness, $F(d,h)$, the form factor $P(K,F)$ is obtained by integrating over $P(K)$ of all constituent particles[7]

$$P(K,F) = \frac{\int_0^\infty \int_0^\infty V_p^2 F(d,h) P(K) \mathrm{d}d\mathrm{d}h}{\int_0^\infty \int_0^\infty V_p^2 F(d,h) \mathrm{d}d\mathrm{d}h} \quad (2)$$

Here, V_p is the volume of the particles.

In the calculation, we set $n = 1.3325$, and $\lambda = 6.328 \times 10^{-7}$ m^{-1}. To taking into account the polydispersity of the disk, we fix the average particle diameter at d_0, the value obtained by laser light scattering (LLS) analysis. For $F(d)$ in eq. (2), we adopted a Gaussian distribution $F(d) = \frac{1}{\sigma\sqrt{2\pi}} \exp\left(-\frac{(d-d_0)^2}{2\sigma^2}\right)$, where the standard deviation σ is arbitrarily set as $\sigma = \sqrt{50}$.

In vitro serum stability analysis. Förster resonance energy transfer (FRET) method was employed to examine the serum stability of four types of nanostructures. Firstly, PEG_{45}-*b*-$PCPTM_{52}$ (2.0 mg), DiO (20 μg), and Dil (20 μg) were dissolved in 1 mL cosolvent, deionized water was then added into the polymer solution at a specified rate. FRET pair-loaded nanostructure dispersions were dialyzed against deionized water and concentrated by ultrafiltration for subsequent studies. The stability of freshly prepared nanostructures at a final concentration of 0.1 g/L was investigated at 37 °C and pH 7.4 under gentle agitation in the presence of pure 10 mM PBS, 45 g/L BSA, or 90v/v% FBS, respectively. Time-resolved fluorescence spectra were measured over 48 h with the excitation wavelength set at 484 nm. The disassembly of nanostructures will lead to the dramatic shift of emission peaks from ~577 nm to ~514 nm (Figure S18 a). The FRET intensity ratio, $I_{577}/(I_{577}+I_{514})$, was utilized to monitor the relative emission peak intensity shift between I_{514} (emission peak of DiO) and I_{577} (the emission peak of Dil). DMF (40-fold by volume) was then added to the nanostructure dispersions, leading to the complete disassembly of nanostructures and the calculation of control FRET intensity ratio. For the quantitative evaluation of data, all recorded FRET ratios were normalized to the initial FRET intensity ratio at t =0 h and the FRET ratio recorded for DMF-treated nanostructures. Residual nanostructure fractions (RNF%) were calculated as follows:

$$\mathrm{RNF\%} = [FRET\ Ratio_{t=\ x\ h} - FRET\ Ratio_{DMF}] / [FRET\ Ratio_{t=0\ h} - FRET\ Ratio_{DMF}] \times 100\%$$

where $FRET\ Ratio_{t=\ x\ h}$, $FRET\ Ratio_{t=0\ h}$, and $FRET\ Ratio_{DMF}$ refer to the FRET ratios at t=

x h, t = 0 h, and FRET ratio recorded for DMF-treated nanostructure dispersion, respectively.

In vitro drug release from polymeric assemblies of polyprodrug amphiphiles. Four types of nanostructures including spheres, smooth disks, large compound vesicles and staggered lamellae self-assembled from PEG_{45}-*b*-$PCPTM_{52}$ polyprodrug amphiphiles were obtained. Polymeric nanoparticles (0.1 g/L) were dispersed in 10 mM PBS buffer at pH 7.4 (0 mM DTT, 2 μM DTT, 5 mM DTT, or 10 mM DTT) and transferred to a dialysis tube (molecular weight cutoff: 3,500 Da) immersed in the same buffered media at 37 ^{o}C respectively. Periodically, aliquots of the external medium were withdrawn and replaced with the same volume of fresh buffer solution. HPLC was employed to assay CPT content to determine the CPT release rate. The drug loading content (DLC%) was calculated as

$$\text{DLC\%} = [W_{\text{conjugated}}]/[W_{\text{polyprodrug}}] \times 100\%$$

where $W_{\text{conjugated}}$ and $W_{\text{polyprodrug}}$ refer to the weights of drug conjugated and polyprodrug amphiphiles, respectively. The actual DLC% of PEG-*b*-PCPTM polyprodrug amphiphiles determined by ^{1}H NMR analysis is shown in Table 1.

The loading content of Dox·HCl in large compound vesicles fabricated from PEG_{45}-*b*-$PCPTM_{52}$ was determined to be 22.3 wt% via HPLC analysis at the wavelength of 485 nm. The Dox·HCl release profile from large compound vesicles was performed under the same condition as in vitro delivery of CPT.

Cellular internalization and intracellular trafficking of nanostructures observed with Confocal Laser Scanning Microscopy (CLSM). HepG2 cells were plated onto glass-bottom petri dishes at a density of 80,000 cells per dish, then cultured in Dulbecco's modified Eagle medium (DMEM) supplemented with 10% fetal bovine serum (FBS), penicillin (100 units/mL), and streptomycin (100 μg/mL) for 24 h at 37 ºC in CO_2/air (5:95). Four types of self-assembled nanostructures obtained from PEG_{45}-*b*-$PCPTM_{52}$ polyprodrug amphiphiles were added at a final CPT-equivalent concentration of 10 μg/mL, respectively. After incubating for 30 min, 1 h, 2 h, 3 h, or 4 h, cells were washed with cold PBS for more than three times. The images were taken using a confocal laser scanning microscopy (Leica TCS SP5 microscope). The blue fluorescence of polymeric assemblies from CPT moieties was observed using a 405 nm laser with the emission channel set to be 420-470 nm. The internalization kinetics of four kinds of nanostructures was estimated by quantifying the blue

fluorescence intensity from fluorescence micrographs. The results were expressed as mean and standard deviation obtained from 50 cells and repeated three times.

To interrogate the endosomal escape ability and intracellular trafficking of four types of nanostructures, late endosomes and lysosomes were stained with Lysotracker Red at 200 nM after incubation with cells for 30 min before imaging and observed using a 594 nm laser, and the emission wavelength was read from 605 to 720 nm and expressed as red. The mitochondria were stained with Mitotracker Green after incubation with cells for 30 min before imaging and observed using a 488 nm laser, and the emission wavelength was read from 500 to 560 nm and expressed as green. The intracellular distribution of polymeric assemblies of PEG_{45}-*b*-$PCPTM_{52}$ polyprodrug amphiphile was quantitatively evaluated by calculating the colocalization ratio of blue fluorescence pixels from PEG_{45}-*b*-$PCPTM_{52}$ with Lysotracker Red pixels and Mitotracker Green pixels. Colocalization ratio of PEG_{45}-*b*-$PCPTM_{52}$ polyprodrug amphiphiles with organelles was quantified as

$$Colocalization\ Ratio\% = [pixels_{colocalization} / pixels_{polyprodrug\ total}] \times 100\%$$

where $pixels_{colocalization}$ represents the number of PEG_{45}-*b*-$PCPTM_{52}$ pixels colocalizing with Lysotracker Red or Mitotracker Green, and $pixels_{polyprodrug\ total}$ represents the number of all the PEG_{45}-*b*-$PCPTM_{52}$ pixels in cells. The results are presented as the mean and standard error of the mean obtained from 50 cells and repeated three times.

The inhibition studies of endocytosis were performed as follows. For the inhibition of energy-dependent endocytosis, HepG2 cells or A549 cells were treated with 0.1% NaN_3/50 mM 2-deoxyglucose in serum-free DMEM for 1 h, followed by incubation with four types of nanostructures for 1 h at 37 ºC in CO_2/air (5:95).[8] For the inhibitors of methyl β-cyclodextrin (MβCD)[8], cells were pre-incubated in serum-free DMEM containing 5 mM MβCD for 15 min at 37 ºC/5% CO_2. The media were then changed to fresh media containing the inhibitor plus self-assembled nanoparticles and further incubated for 1 h at 37 ºC/5% CO_2. For the inhibition of macropinocytosis,[9] cells were pre-incubated in serum-free DMEM with the 1 mM amiloride for 30 min at 37 ºC/5% CO_2, then treated with four types of nanostructures for 1 h. For the inhibition of clathrin-mediated endocytosis,[10] cells were pretreated with the 225 mM sucrose in serum-free DMEM for 30 min at 37 ºC/5% CO_2 and then treated with four types of nanostructures for 1 h. For all endocytic inhibition tests, after exposure to the respective

inhibitors and self-assembled nanostructures for the desired time, the cells were washed with cold PBS and followed by quantifying the fluorescence intensity under CLSM. Percent internalization was normalized to particle internalization in the absence of inhibitors. Data are mean values (200 cells, three experiments).

To further assess the intracellular distribution and drug nuclear accumulation ability of PEG_{45}-*b*-$PCPTM_{52}$ polyprodrug amphiphiles, after treating with four types of assemblies for 2 h or 8 h, HepG2 cells were washed with PBS for three times, fixed with 3.7 wt/v% paraformaldehyde for 10 min, washed with 0.1 wt/v% Triton X-100 for three times, and then stained with Actin-Tracker Green and Tubulin-Tracker Red in the presence of 1 wt/v% BSA for 20 min. After washing with PBS for three times, Actin-Tracker Green and Tubulin-Tracker Red were observed using a 488 nm laser and a 543 nm laser with the emission channel set to be 500 to 540 nm and 560 to 620 nm, respectively.

Four types of nanostructures self-assembled from PEG_{45}-*b*-$P(CPTM_{0.99}$-*co*-$NBD_{0.01})_{33}$ were further utilized to selectively demonstrate the intracellular release of CPT drugs from polymer backbones. Upon treating with four types of nanostructures for 2 h or 8 h, HepG2 cells were washed with cold PBS for three times. The nanostructure polymer backbones were observed through the NBD channel using a 488 nm laser, and the emission wavelength was read from 500-560 nm and expressed as green. Emission of CPT moieties was observed using a 405 nm laser with the emission channel was set to be 420-470 nm and expressed as blue. Cell nucleus was stained with DRAQ5^{TM} for 30 min before imaging and observed using a 633 nm laser, and the emission wavelength was read from 660 to 760 nm and expressed as red.

For flow cytometric analysis, HepG2 cells were seeded into 12-well plates at 80,000 cells per well in 0.5 mL of complete DMEM and cultured at 37 ^{o}C in a 5% CO_2 humidified atmosphere for 24 h. After treating with four types of nanostructures self-assembled from PEG_{45}-*b*-$P(CPTM_{0.99}$-*co*-$NBD_{0.01})_{33}$ for 4 h at 37 ^{o}C, the cells were then rinsed twice with cold PBS. After trypsinizing, the cells were washed with cold PBS, centrifuged and dispersed in cold PBS again. The cells were further washed with cold PBS, filtered through 35 μm nylon mesh and subjected to flow cytometric analysis using a BD FACSCalibur flow cytometer with the excitation wavelength set to be 488 nm for NBD channel.

In vitro cytotoxicity assay. HepG2 cells were chosen to evaluate the in vitro cytotoxicity of

PEG_{45}-*b*-$PCPTM_{52}$ polyprodrug amphiphiles with different nanostructures via MTT assay. HepG2 cells were first cultured in Dulbecco's modified Eagle medium (DMEM) supplemented with 10% fetal bovine serum (FBS), penicillin (100 units/mL), and streptomycin (100 μg/mL) at 37 ^{o}C in a CO_2/air (5:95) incubator for 2 days. For cytotoxicity assay, HepG2 cells were seeded in a 96-well plate at an initial density of 5000 cells/well in 100 μL of complete DMEM medium. After incubating for 24 h, DMEM was replaced with fresh medium, and the cells were treated with self-assembled nanostructures at varying concentrations. The treated cells were incubated in a humidified environment with 5% CO_2 at 37 ^{o}C for 36 h. The MTT reagent (in 20 μL PBS, 5 mg/mL) was added to each well. The cells were further incubated for 4 h at 37 ^{o}C. The medium in each well was then removed and replaced by 180 μL DMSO. The plate was gently agitated for 15 min before the absorbance at 570 nm was recorded by a microplate reader. Each experiment condition was done in quadruple and the data are shown as the mean value plus a standard deviation (± SD).

In vivo blood circulation experiments. Healthy male rats (~300 g, 10 weeks old) were purchased from Experimental Animal Center of Anhui Medical University. All animals received care in compliance with the guidelines outlined in *the Guide for the Care and Use of Laboratory Animals* and all procedures were approved by the Animal Care and Use Committee of University of Science and Technology of China. Four types of nanostructures fabricated from PEG_{45}-*b*-$PCPTM_{52}$ polyprodrug amphiphiles (10 mg CPT-equivalent dose per kg) were injected via the tail vein of rats, respectively. At predetermined time points, orbital vein bleeds (~0.1 mL) were collected into tubes containing heparin and then incubated at 4 ^{o}C. Following the collection of a full set of time points, the rats were sacrificed, plasma was separated from whole blood by centrifuging at 1000 rpm for 10 min. Excess DTT and 9-fold volume of acetonitrile was added to the plasma. The mixtures were vortexed and kept at room temperature for 12 h, followed by quantifying the CPT content by HPLC against the standard curve. Blood circulation half-lives ($t_{1/2}$) were obtained by first-order decay fits. The results were expressed as mean and standard deviation obtained from three rats at each time point and repeated for three times.

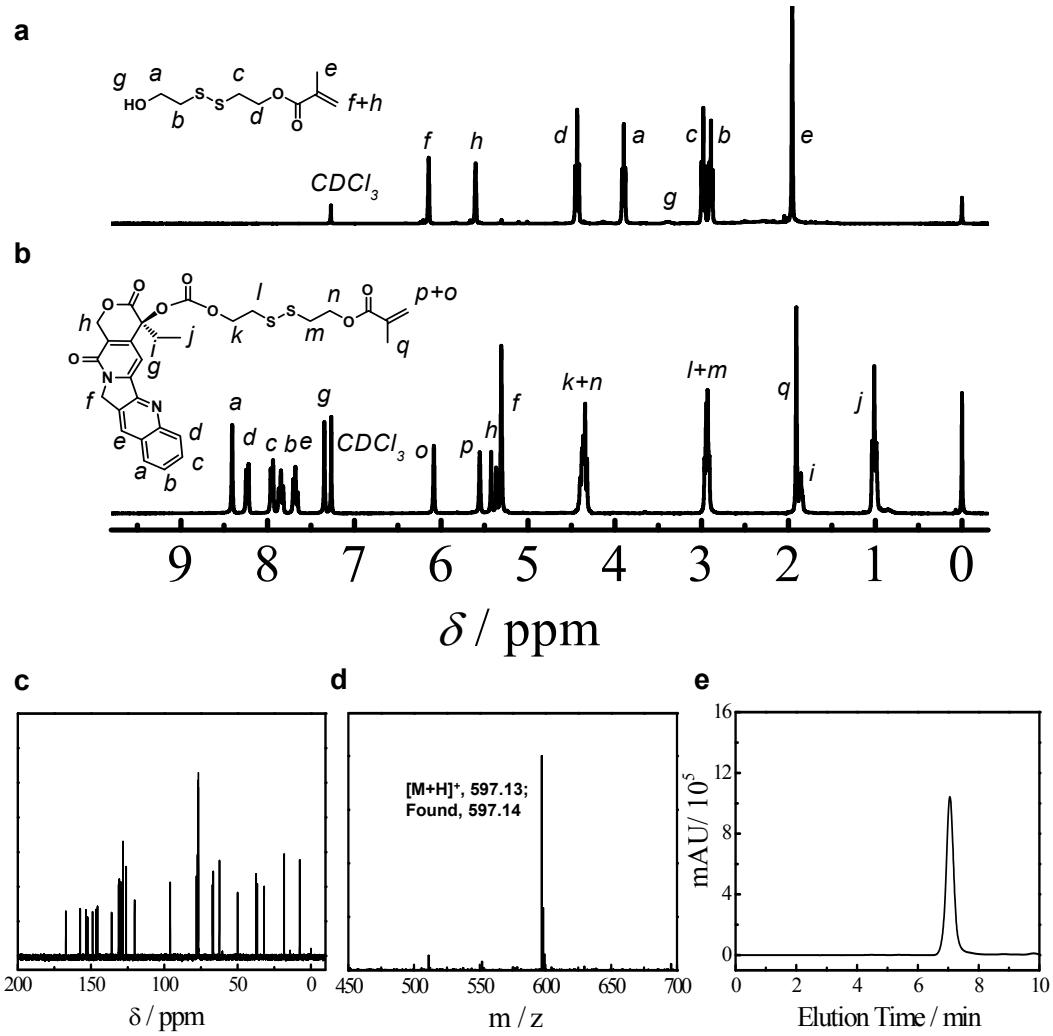

Figure S1. Characterization of reduction-responsive CPT prodrug monomer, CPTM. (a) ^{1}H NMR spectrum of HSEMA. (b) ^{1}H NMR spectrum of CPTM. (c) ^{13}C-NMR spectrum of CPTM recorded in $CDCl_3$. (d) APCI-MS spectrum of CPTM. (e) RP-HPLC trace of CPTM, the mobile phase was 80/20 methanol and water at a flow rate of 1.0 mL/min.

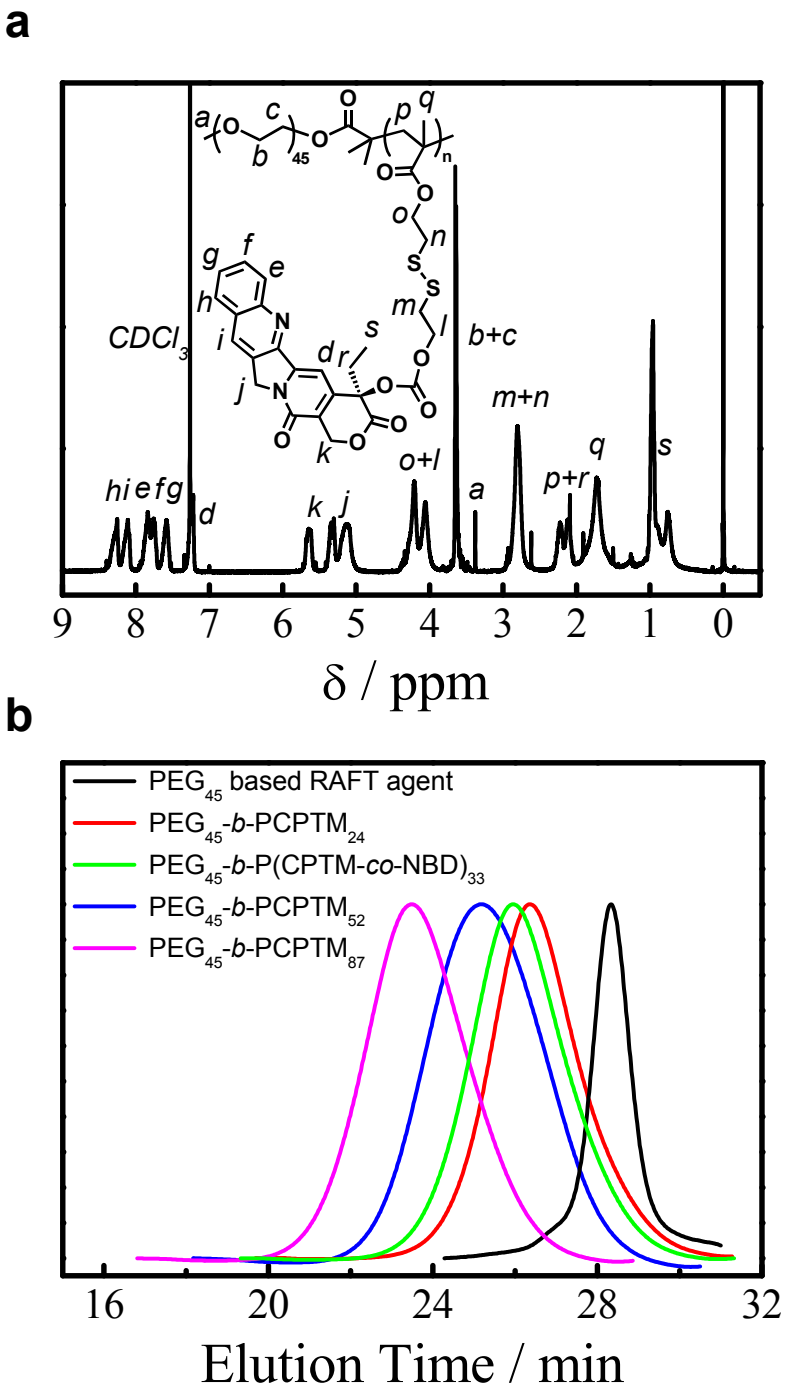

Figure S2. Characterization of PEG-*b*-PCPTM polyprodrug amphiphiles. (a) ^{1}H NMR spectrum recorded for PEG_{45}-*b*-$PCPTM_{52}$ in $CDCl_3$. (b) DMF GPC traces recorded for a series of polyprodrug amphiphiles.

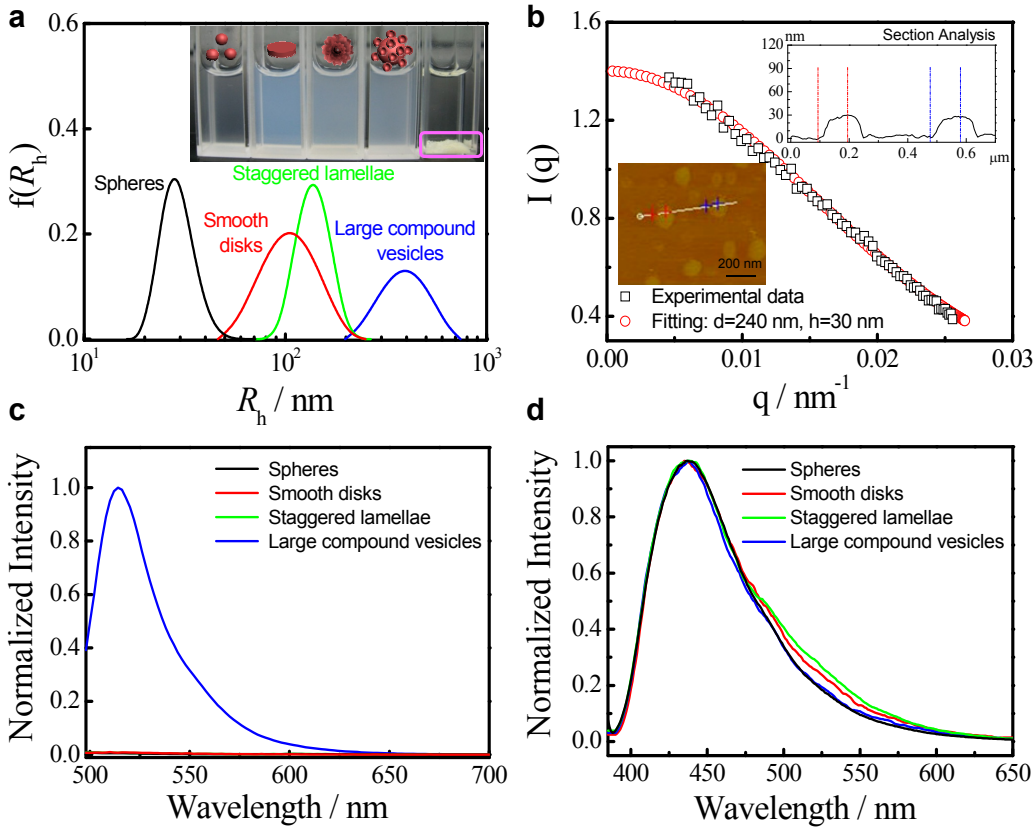

Figure S3. Dynamic laser scattering (DLS), AFM, form factor fitting, and fluorescence spectroscopy characterization of self-assembled nanostructures of PEG_{45}-b-$PCPTM_{52}$. (a) Hydrodynamic radius distributions recorded for 0.15 g/L aqueous dispersion of nanostructures including spheres, smooth disks, staggered lamellae, and flower-like large compound vesicles (Inset: photographs from left to right are the nanoparticle dispersions, the rightmost one is a macroscopic image after treating with DTT, and CPT drug sediments are clearly visible). (b) Static light scattering results of smooth disks. Experimental observations (□) and the best-fit form factor (○) for the smooth disk nanostructure are presented. (Inset: AFM height image with the section analysis of smooth disks). (c) Normalized fluorescence emission spectra recorded for four types of nanostructures, which were self-assembled in 0.1 mM calcein aqueous solution and then subjected to repeated ultrafiltration at pH 7.4 to remove un-encapsulated calcein in the bulk aqueous phase (λ_{ex} = 490 nm). (d) Normalized fluorescence emission spectra recorded for the four types of nanostructures (λ_{ex} = 370 nm).

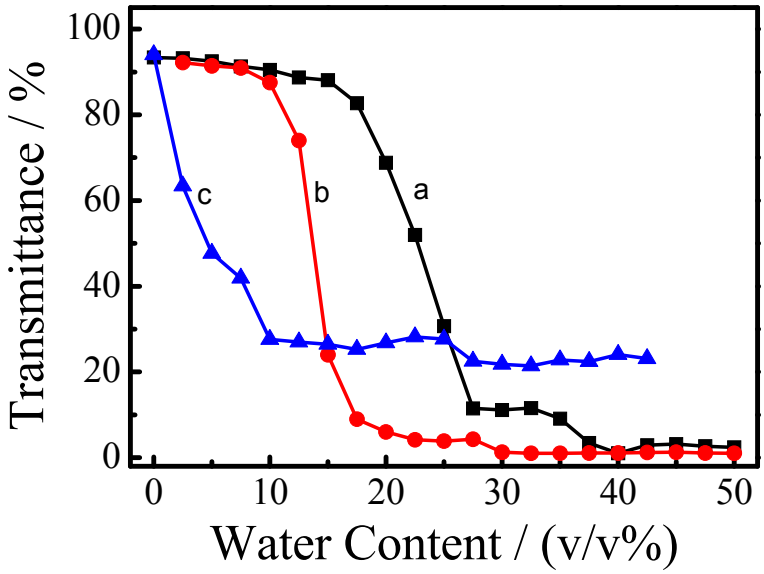

Figure S4. Critical water content determinations for three types of nanostructures during their formation processes. The variation of optical transmittance at 800 nm recorded for 2.0 g/L PEG_{45}-*b*-$PCPTM_{52}$ in 1,4-dioxane upon water addition at different rates. (a) 8 mL/h, affording staggered lamellae. (b) 0.5 mL/h, affording flower-like large compound vesicles. (c) 2.0 g/L PEG_{45}-*b*-$PCPTM_{52}$ in DMSO upon water addition at a rate of 8 mL/h, affording smooth disks.

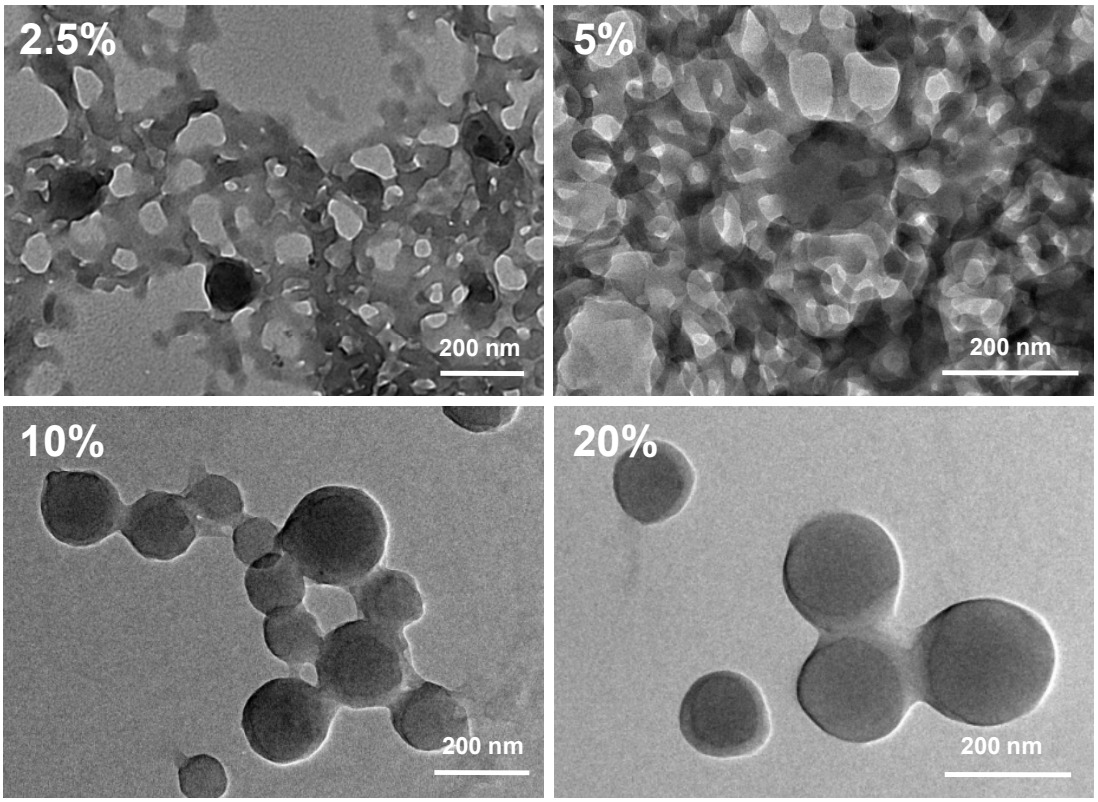

Figure S5. Microstructural evolution of nanostructures with varying water contents during the formation of smooth disks. TEM images were recorded at varying intermediate water contents when deionized water was added into PEG_{45}-*b*-$PCPTM_{52}$ solution in DMSO (2.0 g/L) at a rate of 8 mL/h, this was followed by further stirring for 30 min at room temperature.

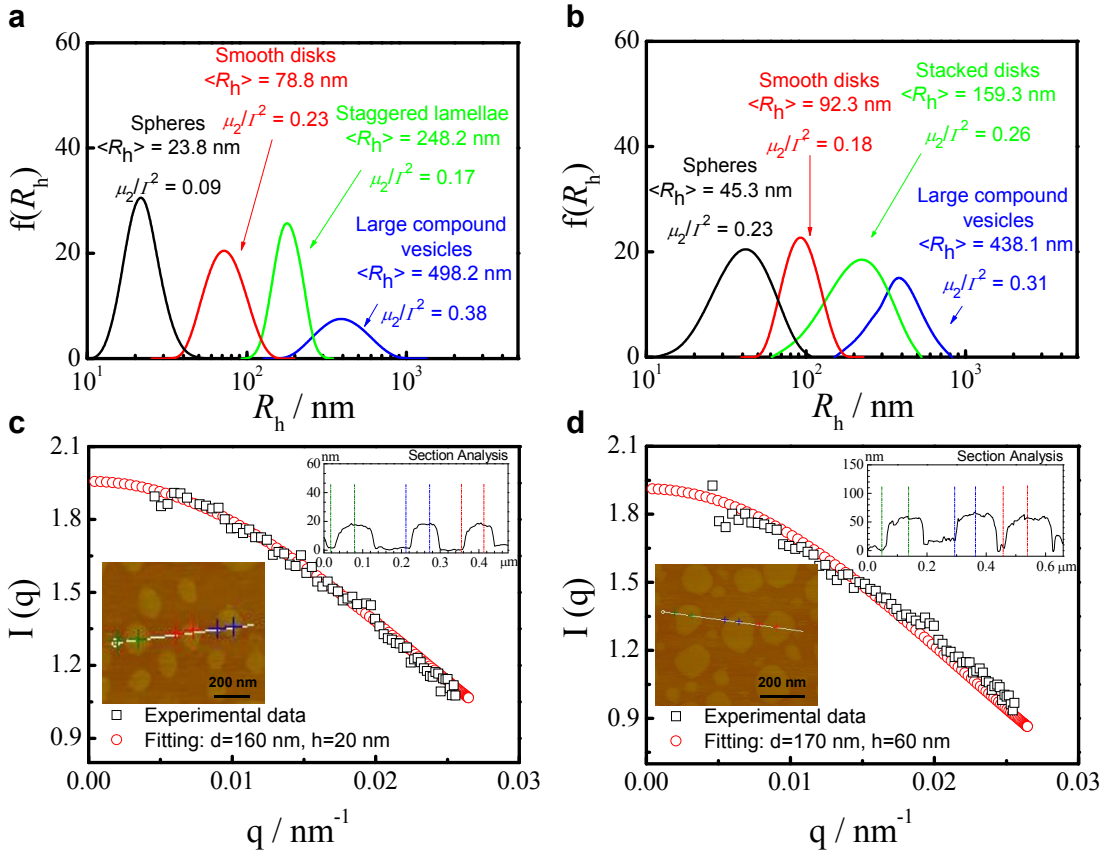

Figure S6. Hydrodynamic radius distributions of four types of nanostructures and static light scattering results and AFM analysis of smooth disk nanostructures of PEG_{45}-*b*-$PCPTM_{24}$ and PEG_{45}-*b*-$PCPTM_{87}$. (a) Hydrodynamic radius distributions of four types of nanostructures of PEG_{45}-*b*-$PCPTM_{24}$. (b) Hydrodynamic radius distributions of four types of nanostructures of PEG_{45}-*b*-$PCPTM_{87}$. (c) and (d) Static light scattering results of smooth disks fabricated from PEG_{45}-*b*-$PCPTM_{24}$ and PEG_{45}-*b*-$PCPTM_{87}$, respectively. Experimental observations (□) and the best-fit form factor (○) for smooth disks are presented (Insets: AFM height images with the section analysis of smooth disks).

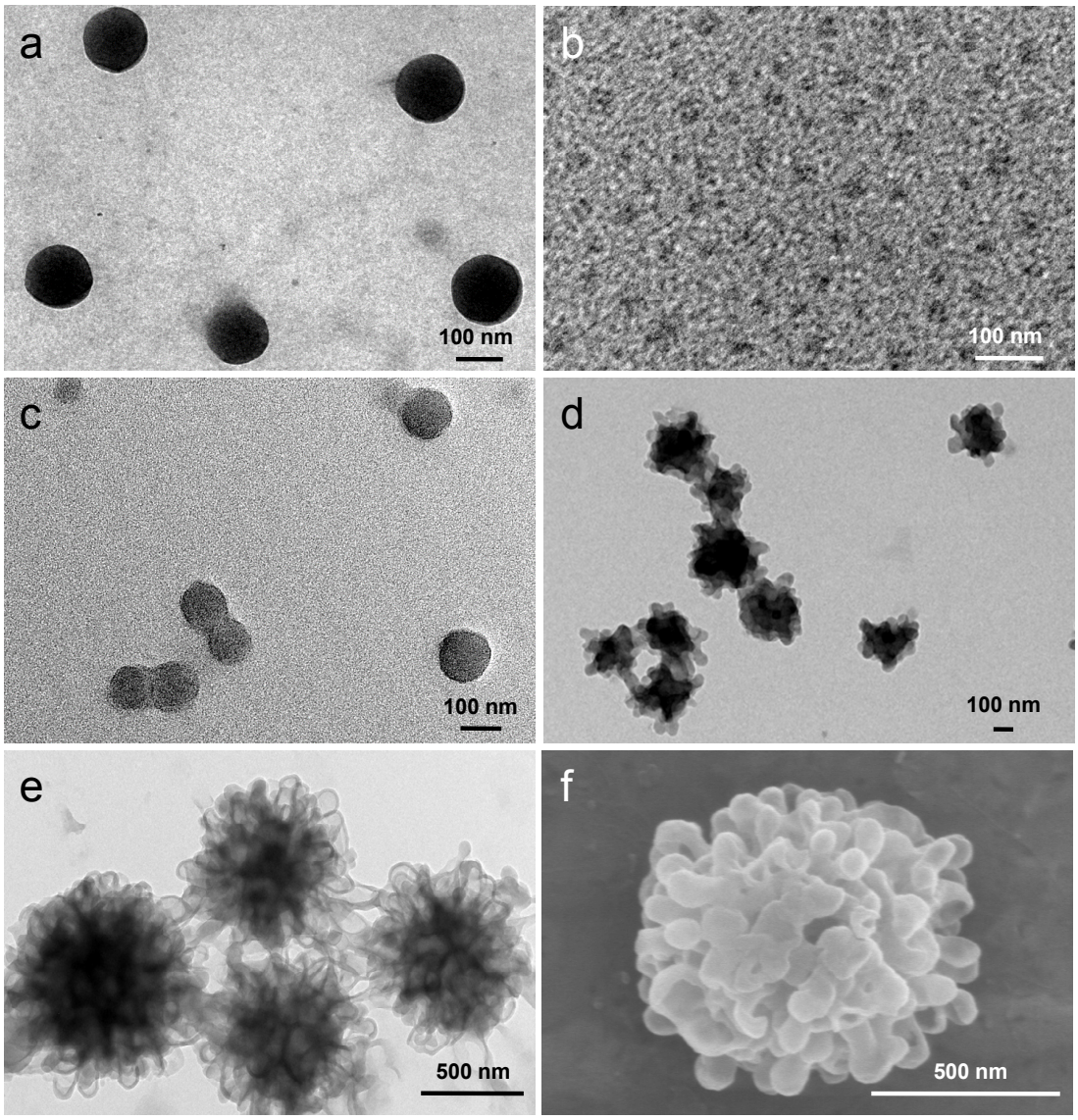

Figure S7. TEM images of (a) well-dispersed smooth disks fabricated from PEG_{45}-*b*-$PCPTM_{87}$ at a final concentration of ~0.04 g/L and (b, c, d and e) four types of nanostructures fabricated from PEG_{45}-*b*-$P(CPTM_{0.99}$-*co*-$NBD_{0.01})_{33}$ by employing the same self-assembling protocols as PEG_{45}-*b*-$PCPTM_{52}$: (b) spheres; (c) smooth disks; (d) staggered lamellae; (e) flower-like large compound vesicles (LCVs); (f) the corresponding SEM image for (e).

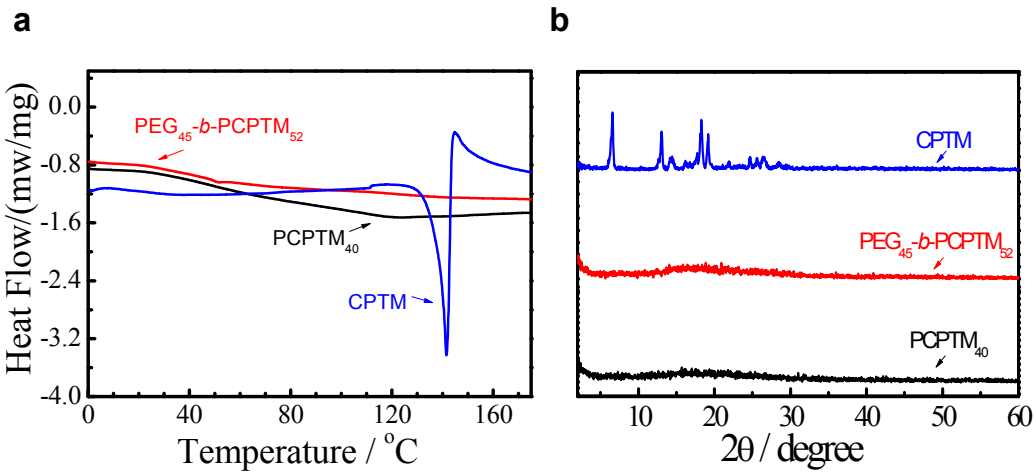

Figure S8. DSC thermograms and XRD spectra analysis. (a) DSC thermograms obtained for PEG_{45}-*b*-$PCPTM_{52}$, CPTM, and $PCPTM_{40}$ homopolymer during the heating process at 10 °C/min. (b) XRD spectra recorded for PEG_{45}-*b*-$PCPTM_{52}$, CPTM, and $PCPTM_{40}$.

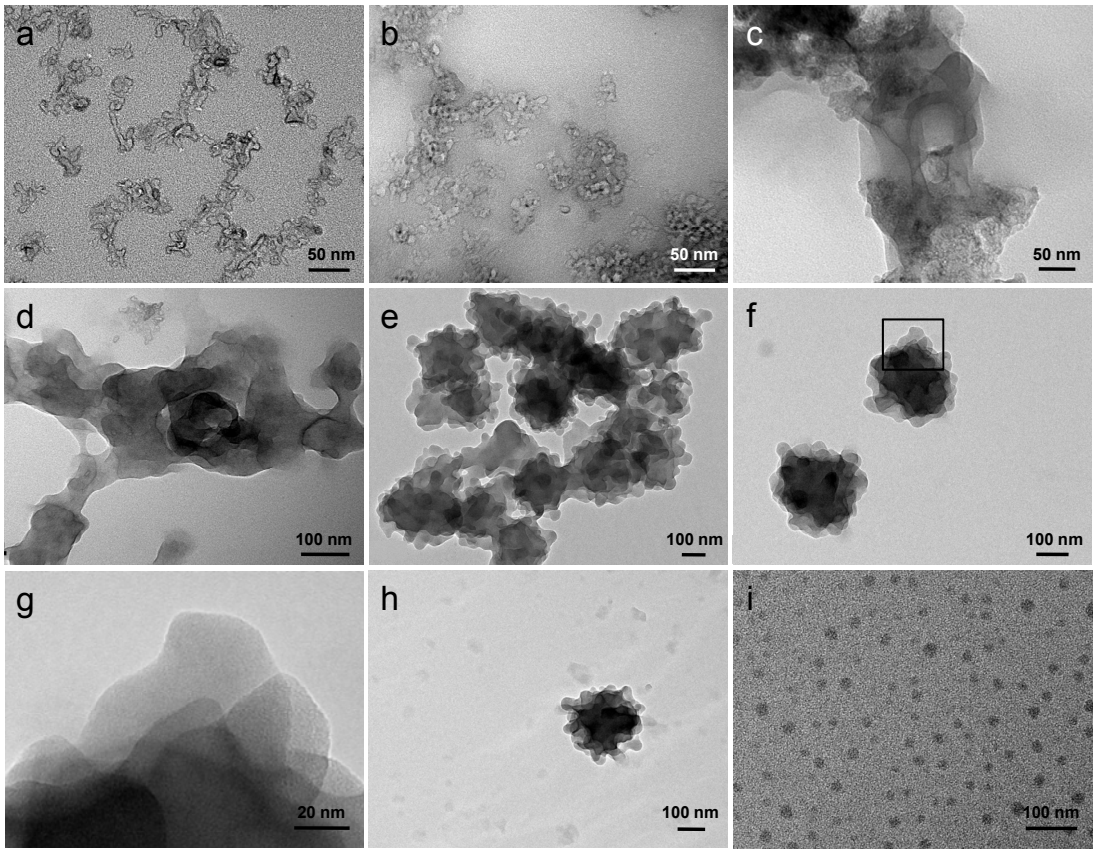

Figure S9. Microstructural evolution of nanostructures with varying water contents during the formation of staggered lamellae. TEM images were recorded at varying intermediate water contents when deionized water was added into PEG_{45}-*b*-$PCPTM_{52}$ solution in 1,4-dioxane (2.0 g/L) at a rate of 8.0 mL/h, this was followed by further stirring for 30 min at room temperature: (a) 10% (v/v). (b) 15% (v/v). (c) 20% (v/v). (d) 30% (v/v). (e) 40% (v/v). (f) 90% (v/v). (g) Close up shot of the spiked edge as indicated in image f. (h) The aqueous dispersion of staggered lamellae after ultrasonication treatment for 15 min. (i) TEM image recorded for the aqueous dispersion of staggered lamellae after ultrasonication treatment for 30 min in the presence of 0.2 g/L Tween-20.

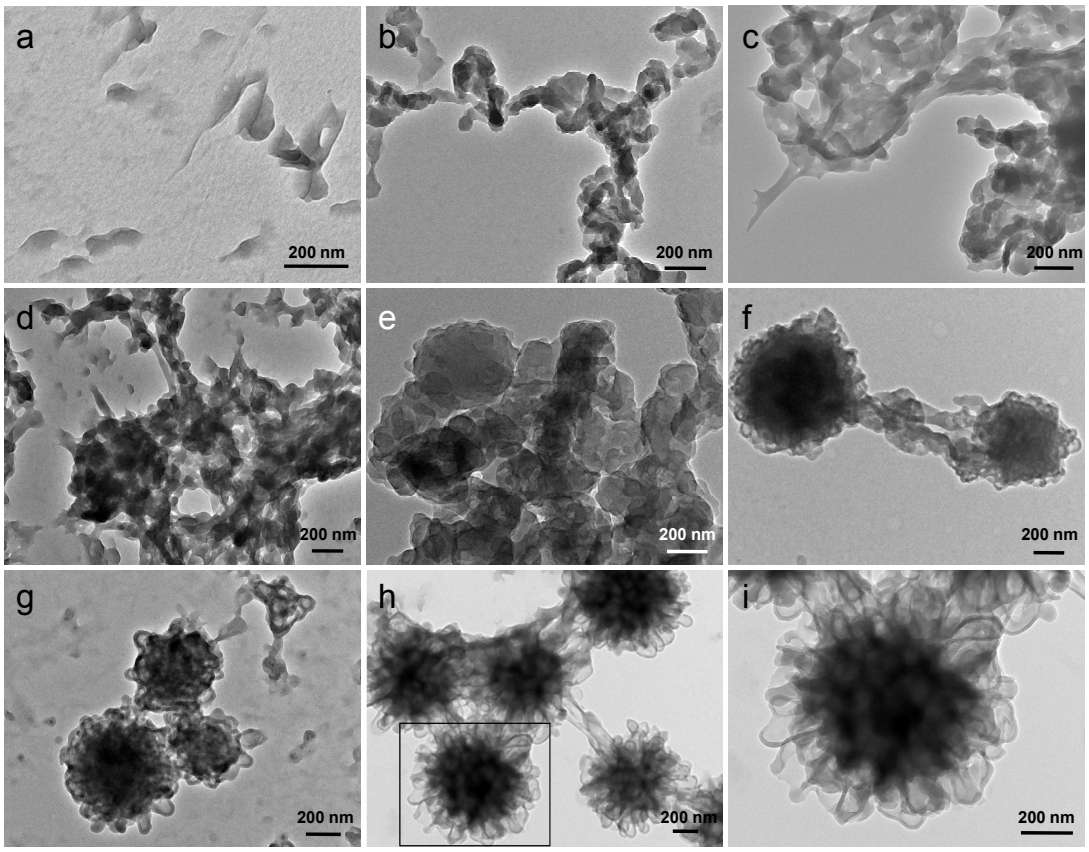

Figure S10. Microstructural evolution of nanostructures with varying water contents during the formation of large compound vesicles. TEM images were recorded at varying intermediate water contents when deionized water was added into PEG_{45}-*b*-$PCPTM_{52}$ solution in 1,4-dioxane (2.0 g/L) at a rate of 0.5 mL/h, this was followed by further stirring for 30 min at room temperature: (a) 5% (v/v). (b) 10% (v/v). (c) 12.5% (v/v). (d) 15% (v/v). (e) 20% (v/v). (f) 30% (v/v). (g) 50% (v/v). (h) 90% (v/v). (i) Close up shot of the indicated region in image h.

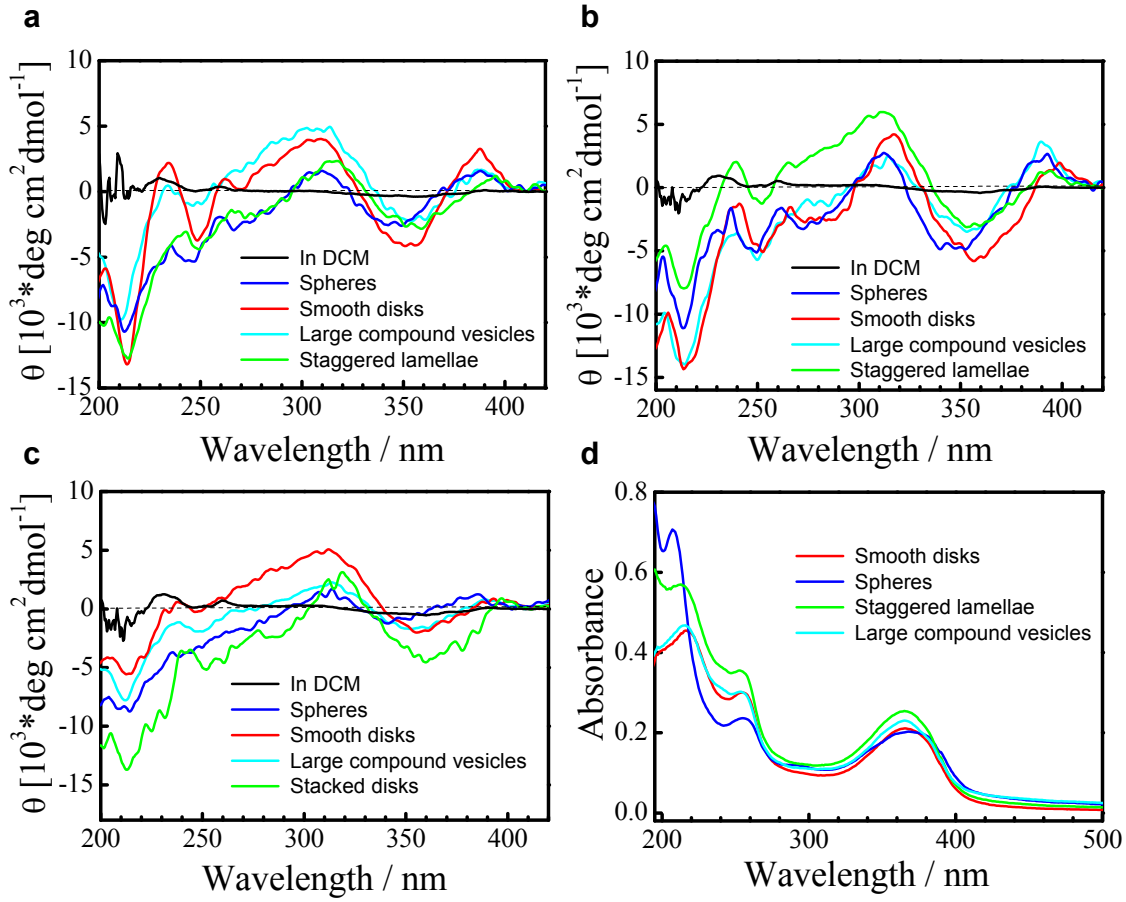

Figure S11. Circular dichroism (CD) and UV-vis absorption spectra analyses. CD spectra recorded for the four types of nanostructures self-assembled from three polyprodrug amphiphiles at a concentration of 0.15 g/L: (a) PEG_{45}-*b*-$PCPTM_{24}$. (b) PEG_{45}-*b*-$PCPTM_{52}$. (c) PEG_{45}-*b*-$PCPTM_{87}$; the CD spectra for molecularly dissolved diblock chains in DCM are also included. (d) UV-vis absorption spectra for four types of nanostructures self-assembled from PEG_{45}-*b*-$PCPTM_{52}$.

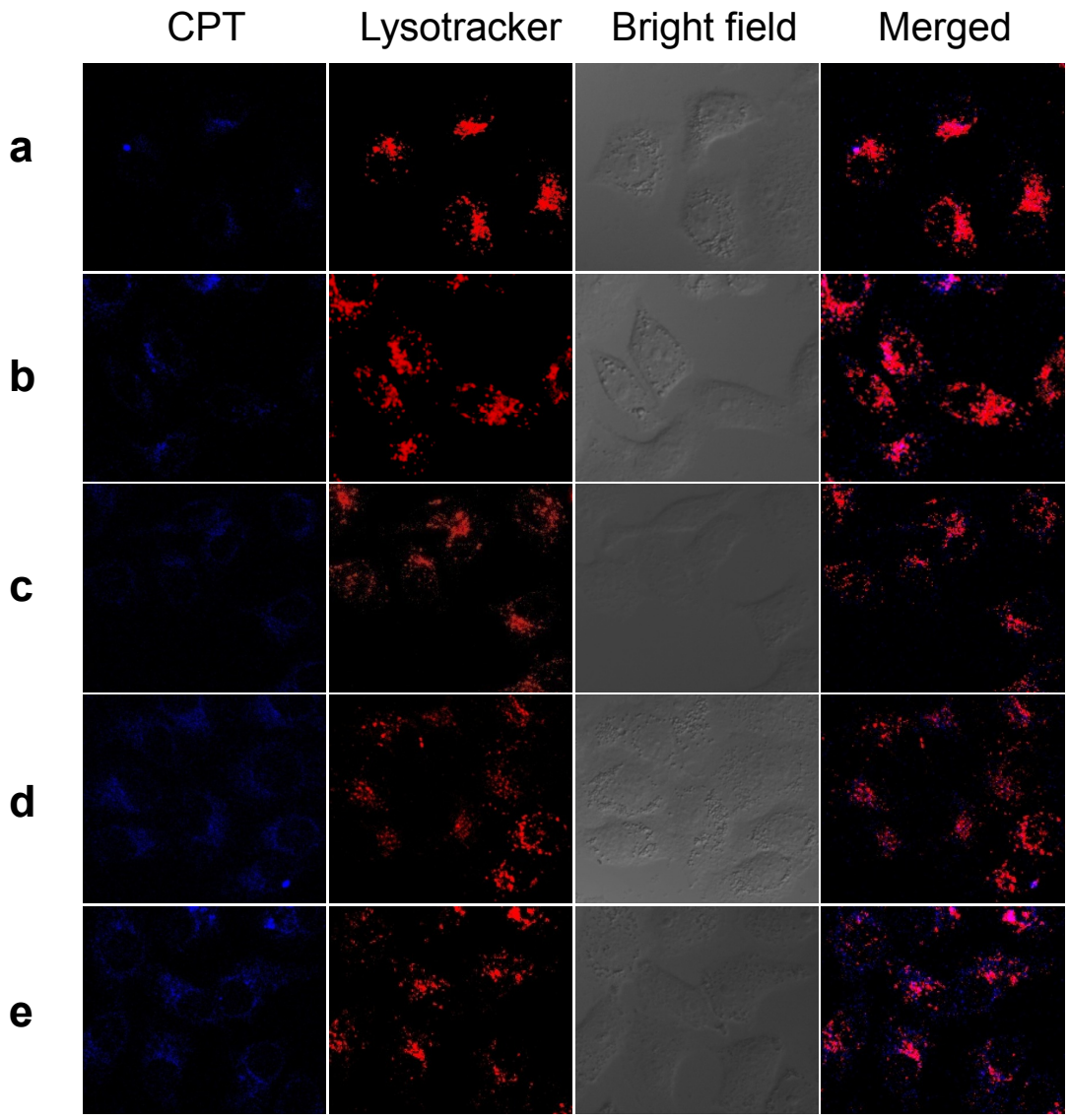

Figure S12. Cellular uptake and colocalization analysis for spheres. CLSM images of HepG2 cells after incubation with spheres fabricated from PEG_{45}-*b*-$PCPT_{52}$ (10 μg/mL CPT-equivalent dosage) at 37 ^{o}C after varying incubation duration. (a) 30 min. (b) 1 h. (c) 2 h. (d) 3 h. (e) 4 h. Late endosomes and lysosomes were stained with Lysotracker Red (red).

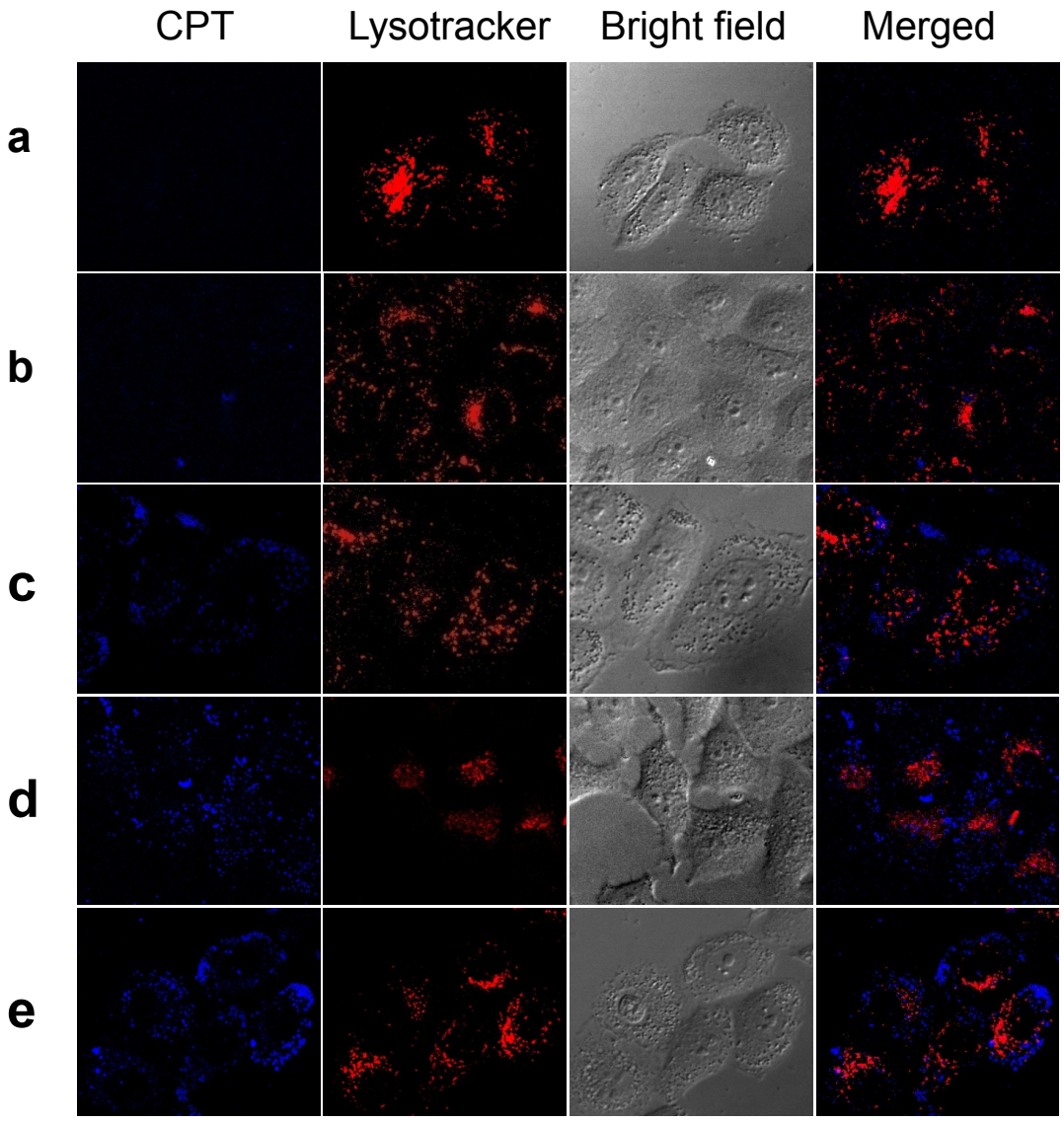

Figure S13. Cellular uptake and colocalization analysis for smooth disks. CLSM images of HepG2 cells after incubation with smooth disks fabricated from PEG_{45}-*b*-$PCPT_{52}$ (10 μg/mL CPT-equivalent dosage) at 37 ^{o}C after varying incubation duration. (a) 30 min. (b) 1 h. (c) 2 h. (d) 3 h. (e) 4 h. Late endosomes and lysosomes were stained with Lysotracker Red (red).

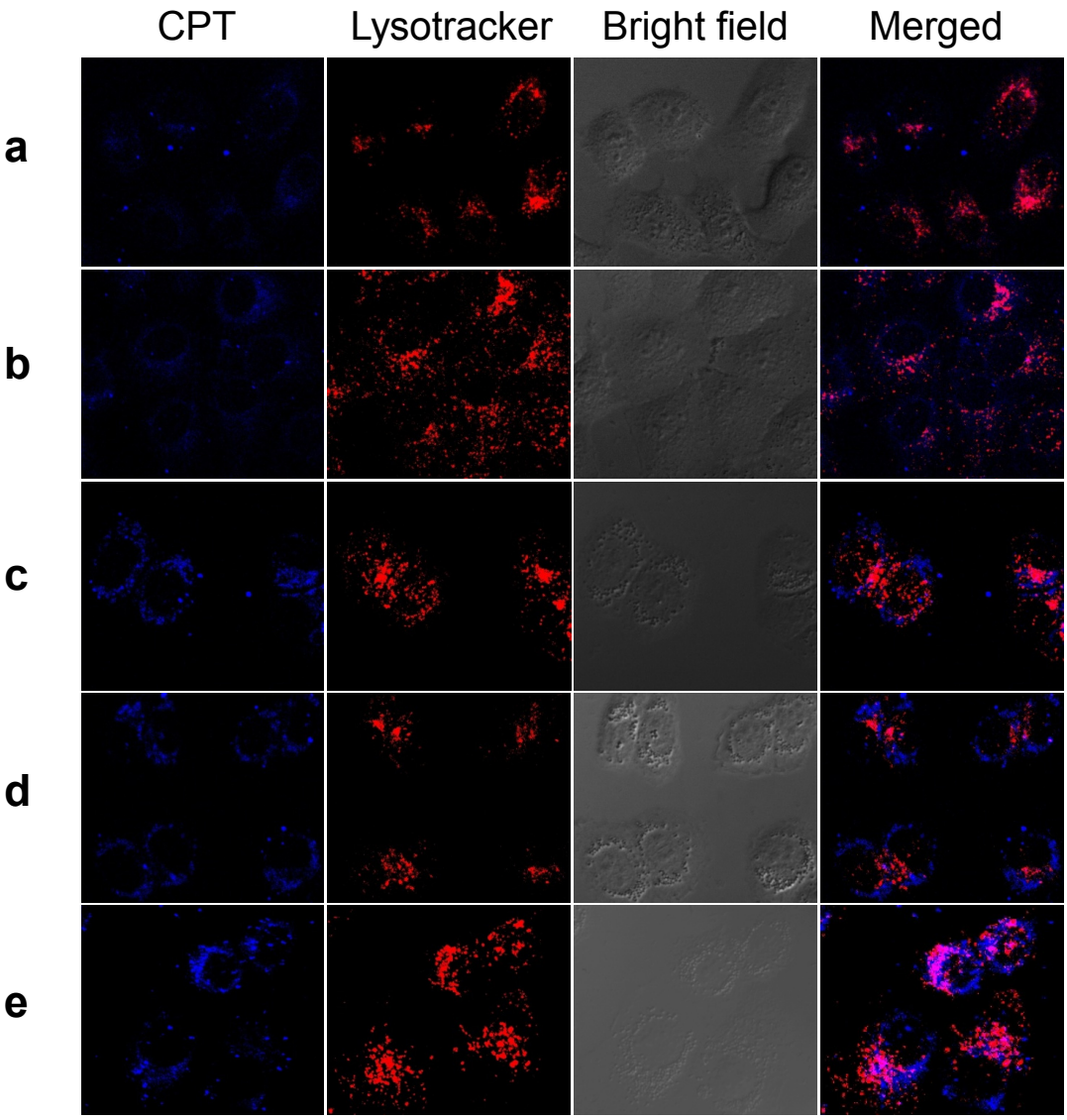

Figure S14. Cellular uptake and colocalization analysis for flower-like large compound vesicles. CLSM images of HepG2 cells after incubation with large compound vesicles fabricated from PEG_{45}-*b*-$PCPT_{52}$ (10 μg/mL CPT-equivalent dosage) at 37 ^{o}C after varying incubation duration. (a) 30 min. (b) 1 h. (c) 2 h. (d) 3 h. (e) 4 h. Late endosomes and lysosomes were stained with Lysotracker Red (red).

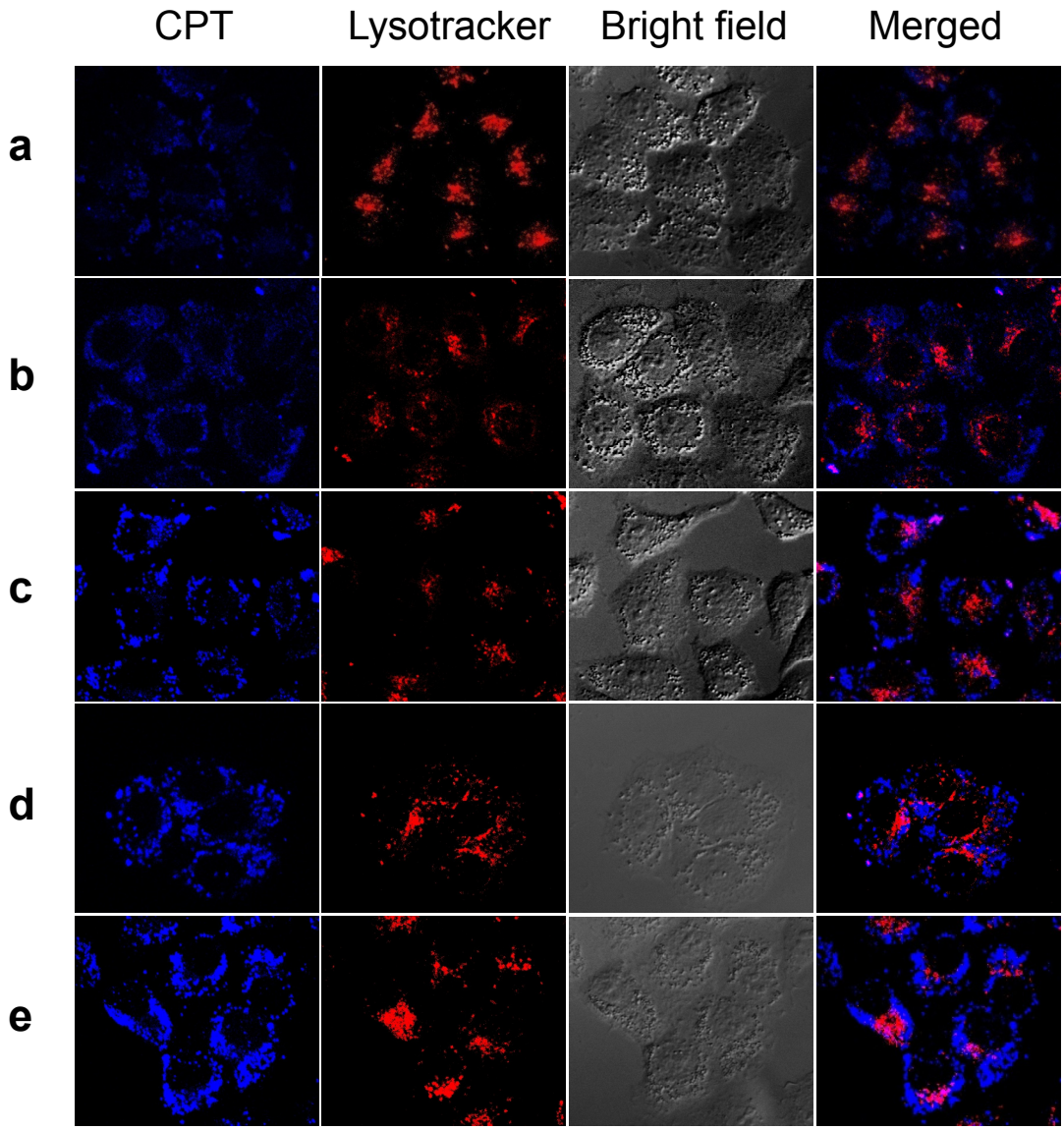

Figure S15. Cellular uptake and colocalization analysis for staggered lamellae. CLSM images of HepG2 cells after incubation with staggered lamellae fabricated from PEG_{45}-*b*-$PCPT_{52}$ (10 μg/mL CPT-equivalent dosage) at 37 °C after varying incubation duration. (a) 30 min. (b) 1 h. (c) 2 h. (d) 3 h. (e) 4 h. Late endosomes and lysosomes were stained with Lysotracker Red (red).

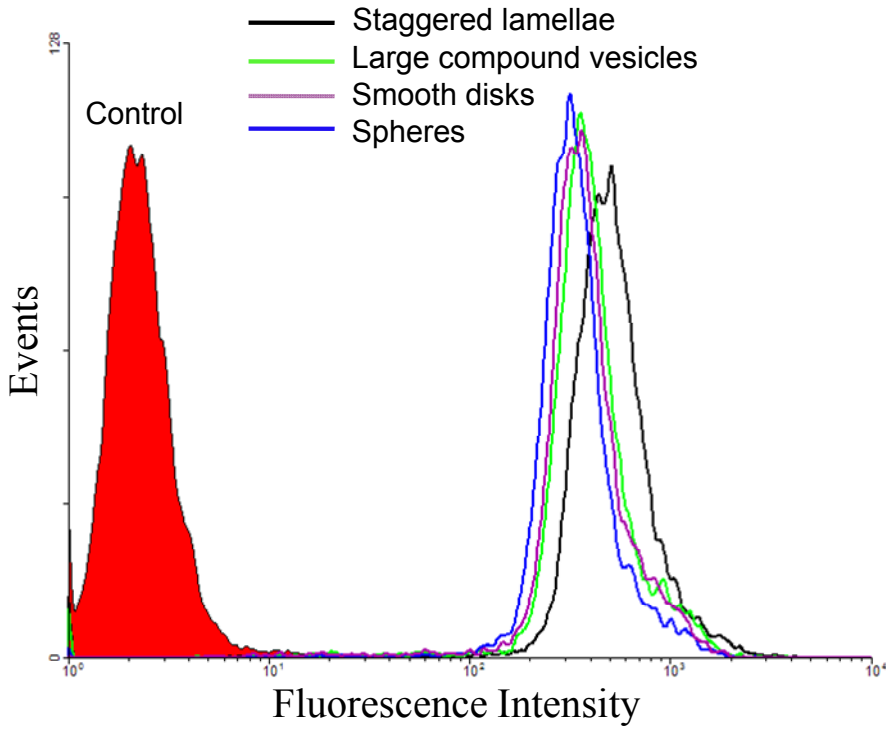

Figure S16. Confirmation of cellular uptake rates by flow cytometric analysis. Flow cytometric analysis recorded for HepG2 cells after 4 h incubation with four types of nanostructures self-assembled from NBD-labeled polyprodrug amphiphiles, PEG-*b*-P(CPT-*co*-NBD), as determined by NBD channel.

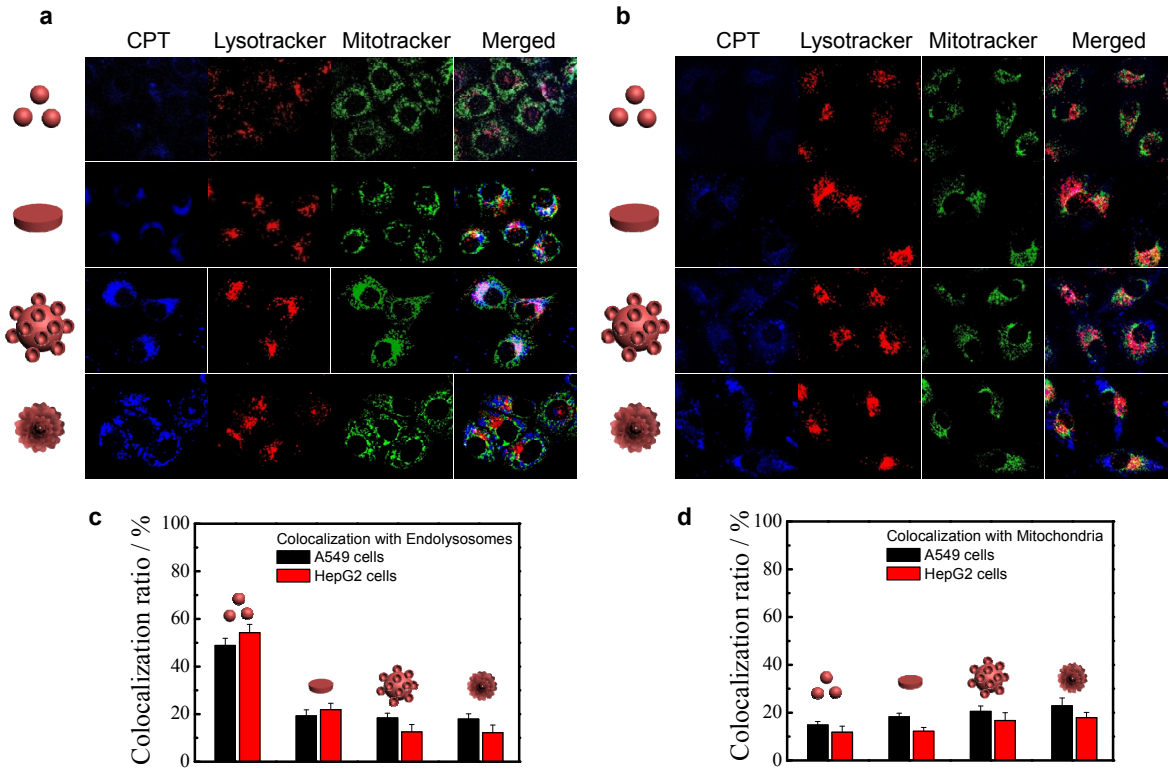

Figure S17. Intracellular localization of four types of nanostructures self-assembled from PEG_{45}-*b*-$PCPTM_{52}$ for HepG2 cells and A549 cells after 4 h incubation. (a) CLSM images of HepG2 cells. (b) CLSM images of A549 cells. (c) Colocalization ratio analysis between blue channel fluorescence from polyprodrug amphiphiles and red fluorescence of stained late endosomes/lysosomes. (d) Colocalization ratio analysis between the blue channel fluorescence and green channel fluorescence of stained mitochondria. The late endosomes/ lysosomes and mitochondria were stained with Lysotracker Red (red) and Mitotracker Green (green), respectively. Data are mean values (~50 cells, three parallel experiments, $p<0.05$).

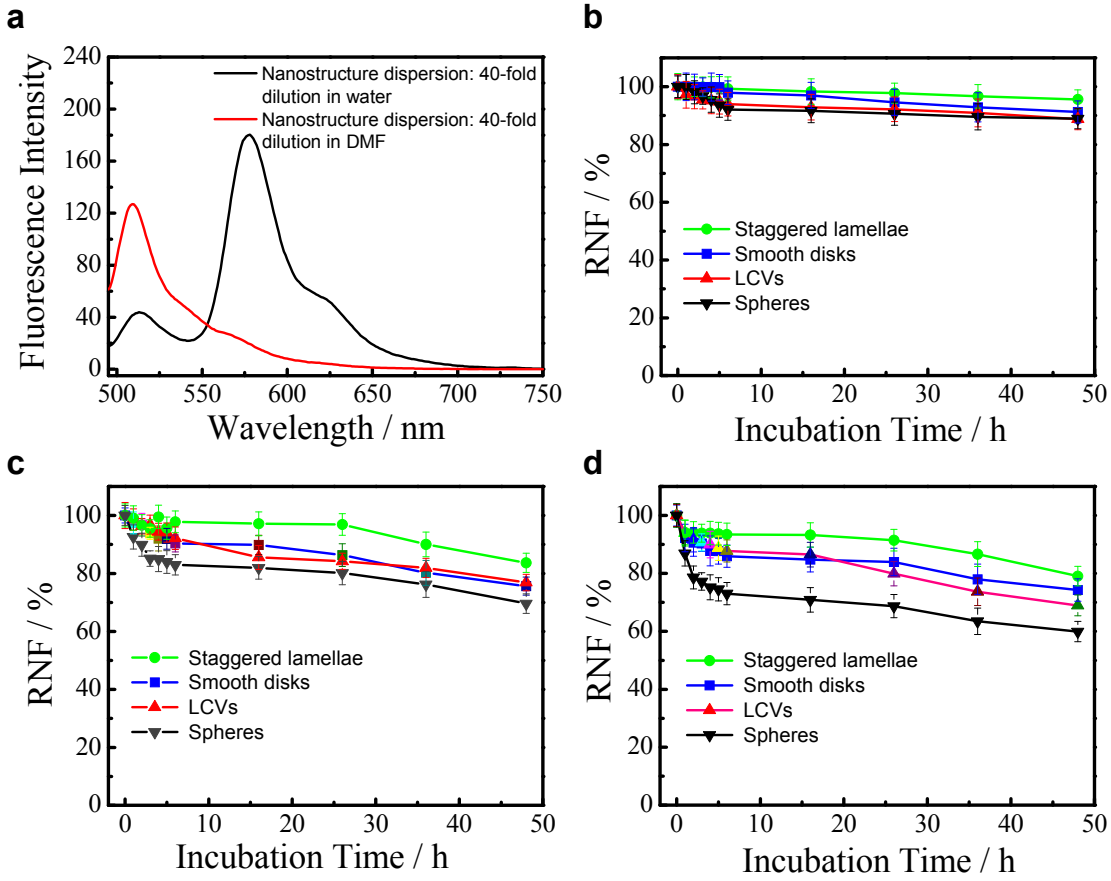

Figure S18. *In vitro* serum stability tests of four types of nanostructures fabricated from PEG_{45}-*b*-$PCPTM_{52}$. (a) Typical fluorescence spectra of DiO and Dil co-loaded nanostructure dispersion upon dilution with 40-fold water or DMF (v/v). Residual nanostructure fractions (RNF%) were determined for four types of nanostructures at 37 ^{o}C and pH 7.4 under gentle agitation in the presence of (b) 10 mM PBS, (c) 45 g/L BSA, and (d) 90 v% FBS (three parallel experiments, P<0.005).

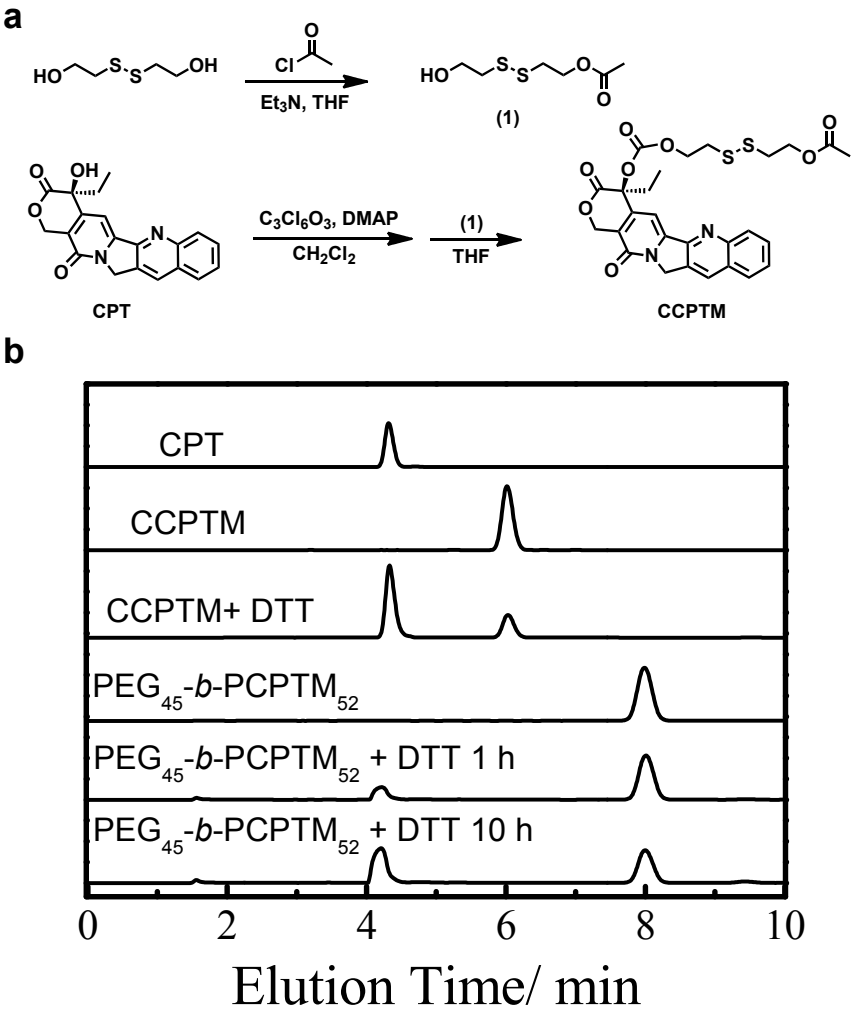

Figure S19. Reduction-responsive CPT release from polyprodrug amphiphiles. (a) Synthetic routes employed for the control prodrug without unsaturated double bonds, CCPTM. (b) RP-HPLC traces recorded for CPT, CCPTM, CCPTM upon treating with DTT, and the aqueous dispersion of PEG_{45}-*b*-$PCPTM_{52}$ upon treatment with DTT at varying time durations. The mobile phase was 80/20 methanol and water at a flow rate of 1.0 mL/min.

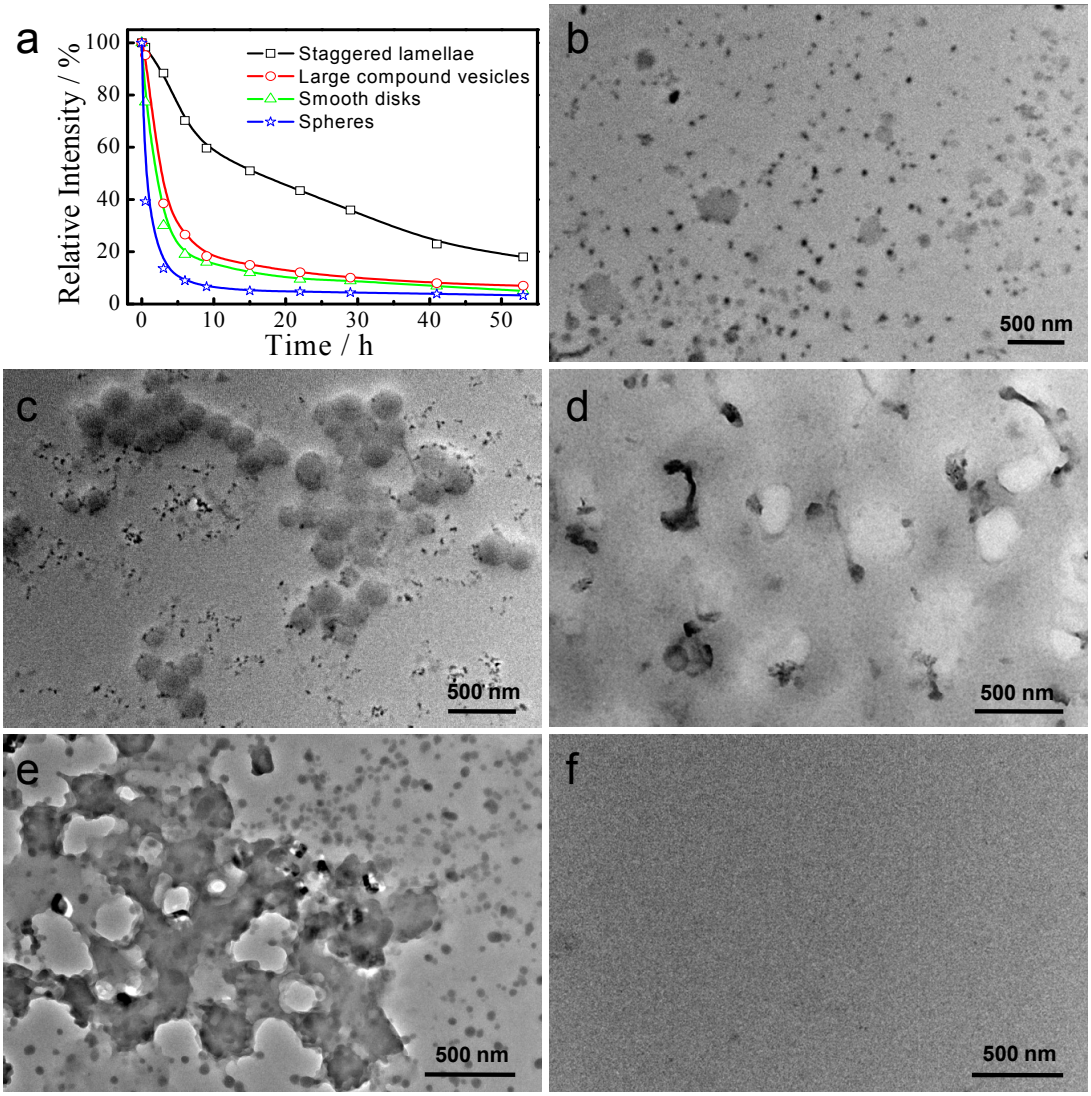

Figure S20. Degradation kinetics for four types of nanostructures of PEG_{45}-*b*-$PCPT_{52}$ as determined by DLS and TEM. (a) Normalized scattered light intensities determined by DLS recorded for assemblies at a concentration of 0.1 g/L upon treating with 10 mM DTT at pH 7.4 and 37 ^{o}C. TEM images were recorded for four types of nanostructures after 6 h incubation upon addition of DTT. (b) Spheres. (c) Smooth disks. (d) Large compound vesicles. (e) Staggered lamellae. (f) is the representative TEM image recorded for staggered lamellae dispersion after ~100 h incubation with 10 mM DTT.

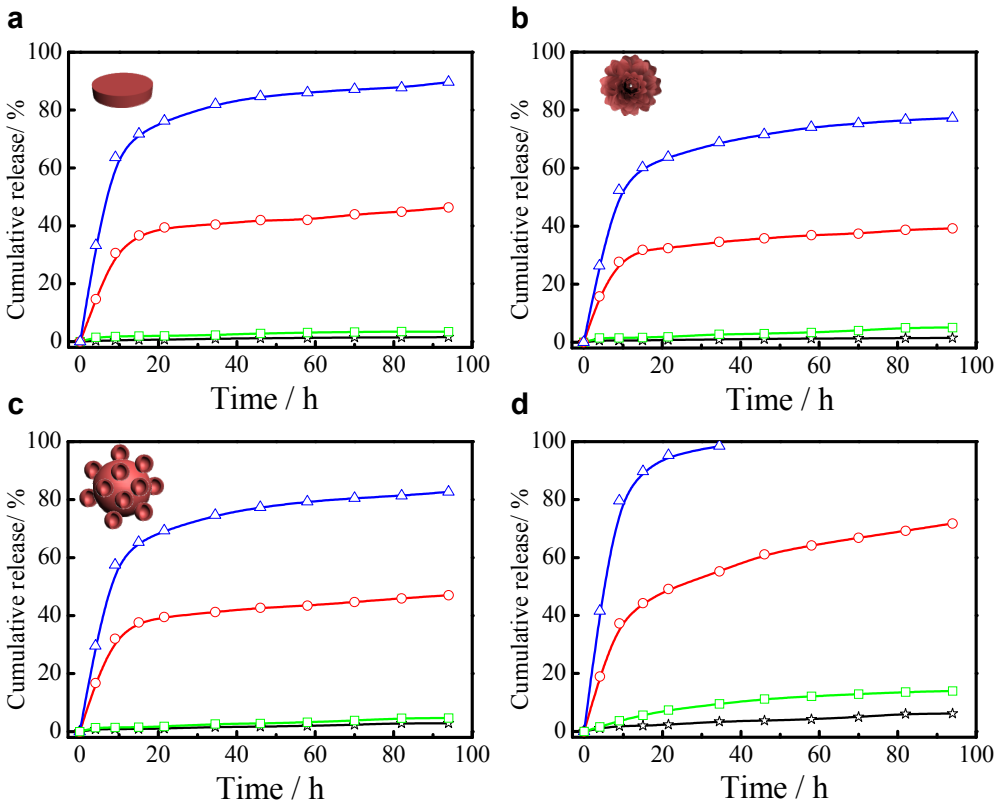

Figure S21. In vitro drug release profiles from distinct nanostructures of PEG_{45}-*b*-$PCPTM_{52}$. CPT release profiles recorded at pH 7.4 and 37 ^{o}C under different DTT concentrations (☆) 0 mM DTT, (□) 2 μM DTT, (○) 5 mM DTT and (△) 10 mM DTT: (a) Smooth disks. (b) Staggered lamellae. (c) Large compound vesicles. (d) Dox·HCl release kinetics from Dox·HCl-loaded large compound vesicles.

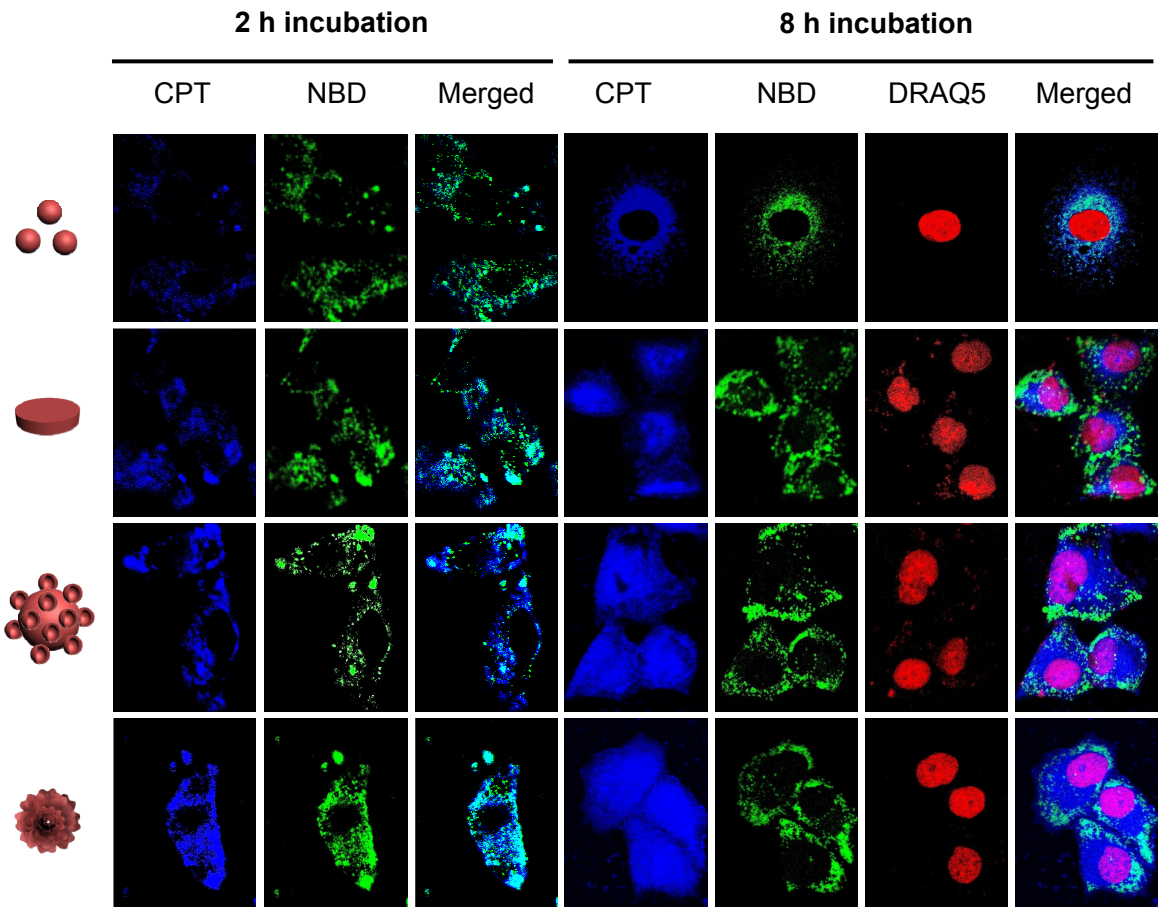

Figure S22. CLSM images for the determination of intracellular distribution of CPT moieties (blue channel) and nanostructured polymer backbones in HepG2 cells upon 2 h and 8 h incubation with four types of nanostructures fabricated from NBD-labeled PEG_{45}-*b*-$P(CPTM_{0.99}$-*co*-$NBD_{0.01})_{33}$ diblock copolymer. NBD (green channel) was utilized to label polymer backbones. DRAQ5™ (red) was employed to stain cell nucleus.

Supplementary References

(1) Liu, T.; Liu, S. Y. *Anal. Chem.* **2011**, *83*, 2775-2785.

(2) Uchiyama, S.; Matsumura, Y.; de Silva, A. P.; Iwai, K. *Anal. Chem.* **2003**, *75*, 5926-5935.

(3) Boyer, C.; Bulmus, V.; Davis, T. P.; Ladmiral, V.; Liu, J. Q.; Perrier, S. *Chem. Rev.* **2009**, *109*, 5402-5436.

(4) Hu, X.; Tian, J.; Liu, T.; Zhang, G.; Liu, S. *Macromolecules* **2013**, *46*, 6243-6256.

(5) Guinier, A.; Fournet, G. *Small Angle Scattering of X-rays; John Wiley and Sons: New York* 1955.

(6) van der Kooij, F. M.; Philipse, A. P.; Dhont, J. K. G. *Langmuir* **2000**, *16*, 5317-5323.

(7) Dhont, J. K. G. *An Introduction to the Dynamics of Colloids; Elsevier: Amsterdam*. 1996.

(8) Gratton, S. E. A.; Ropp, P. A.; Pohlhaus, P. D.; Luft, J. C.; Madden, V. J.; Napier, M. E.; DeSimone, J. M. *Proc. Natl. Acad. Sci. U. S. A.* **2008**, *105*, 11613-11618.

(9) Koivusalo, M.; Welch, C.; Hayashi, H.; Scott, C. C.; Kim, M.; Alexander, T.; Touret, N.; Hahn, K. M.; Grinstein, S. *J. Cell Bio.* **2010**, *188*, 547-563.

(10) Rejman, J.; Bragonzi, A.; Conese, M. *Mol. Ther.* **2005**, *12*, 468-474.